Master Thesis

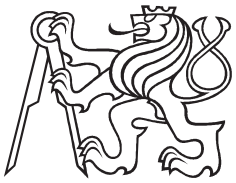

Czech
Technical
University
in Prague

F3

Faculty of Electrical Engineering
Department of Cybernetics

Classification of respiratory system compliance changes during mechanical ventilation using electrical impedance tomography

Lukáš Mařík

Supervisor: Philip von Platen, M.Sc.
Second supervisor: Ing. Jan Havlík, Ph.D.
January 2021

MASTER'S THESIS ASSIGNMENT

I. Personal and study details

Student's name: **Mařík Lukáš** Personal ID number: **434122**

Faculty / Institute: **Faculty of Electrical Engineering**

Department / Institute: **Department of Cybernetics**

Study program: **Biomedical Engineering and Informatics**

Branch of study: **Biomedical Informatics**

II. Master's thesis details

Master's thesis title in English:

Classification of Respiratory System Compliance Changes during Mechanical Ventilation Using Electrical Impedance Tomography

Master's thesis title in Czech:

Klasifikace změn poddajnosti dýchacího systému během mechanické plicní ventilace pomocí elektrické impedanční tomografie

Guidelines:

Mechanical ventilation is a life-saving treatment for patients with acute respiratory failure. However, correctly choosing the ventilator settings is not trivial. A particularly difficult parameter to set is the positive end-expiratory pressure (PEEP) as choosing a PEEP that is too low may cause atelectasis, whilst choosing a PEEP that is too high may cause over distention of the lungs.
The compliance of the respiratory system (based on a single compartment model of the lungs) is a widely used parameter to evaluate different PEEP settings. However, the compliance is only global parameter, meaning local over distension or atelectasis is not visible. The electrical impedance tomography is one method to evaluate the local changes in the lung during ventilation.
The aim of this thesis is therefore to develop a classification algorithm to determine whether the global compliance changes are in fact an improvement based on local information.
The following subgoals are to be considered:
• Literature review
• Measurement data pre-processing (EIT and ventilation curves)
• EIT data processing using EIDORS
• Development of an artificial intelligence algorithm to classify compliance changes
• Statistical analysis of results
• Evaluation of results
• Documentation

Bibliography / sources:

[1] Frerichs, I., Dargaville, P.A., Dudykevych, T. et al. – Electrical impedance tomography: a method for monitoring regional lung aeration and tidal volume distribution? – Intensive Care Med 29, 2312–2316, 2003.
[2] Meier, T., Luepschen, H., Karsten, J. et al. – Assessment of regional lung recruitment and derecruitment during a PEEP trial based on electrical impedance tomography. – Intensive Care Med 34, 543–550, 2008.
[3] Luepschen, H, Meier, T., Grossherr, M. et al. – Protective ventilation using electrical impedance tomography – Physiol. Meas. 28 S247, 2007.
[4] Gómez-Laberge, C. et al. – Data-driven classification of ventilated lung tissues using electrical impedance tomography – Physiol. Meas. 32 903, 2011.
[5] Grychtol, B. et al. – Towards lung EIT image segmentation: automatic classification of lung tissue state from analysis of EIT monitored recruitment manoeuvres – Physiol. Meas. 31 S31, 2010.

Name and workplace of master's thesis supervisor:

Philip von Platen, M.Sc., RWTH Aachen University

Name and workplace of second master's thesis supervisor or consultant:

Ing. Jan Havlík, Ph.D., Department of Circuit Theory, FEE

Date of master's thesis assignment: **15.06.2020** Deadline for master's thesis submission: **05.01.2021**

Assignment valid until: **19.02.2022**

Philip von Platen, M.Sc.	doc. Ing. Tomáš Svoboda, Ph.D.	prof. Mgr. Petr Páta, Ph.D.
Supervisor's signature	Head of department's signature	Dean's signature

III. Assignment receipt

The student acknowledges that the master's thesis is an individual work. The student must produce his thesis without the assistance of others, with the exception of provided consultations. Within the master's thesis, the author must state the names of consultants and include a list of references.

.	
Date of assignment receipt	Student's signature

Acknowledgements

I would like to express my gratitude to the many people involved in the completion of this thesis.

First and foremost, I would like to thank my supervisor Philip von Platen, M.Sc., for his support and encouragement throughout this thesis. His guidance and motivation allowed me to concentrate on the key aspects while providing the occasion to develop my own ideas.

I would like to thank Univ.-Prof. Dr.-Ing. Dr. med. Steffen Leonhardt for the opportunity that the double-degree program offers, and Ing. Jan Havlík, Ph.D. for the inspiration to participate in the program and ultimately the supervision of the thesis at CTU.

A special thanks go to my girlfriend for thorough proof reading and relevant comments.

Finally, I would also like to show my deep appreciation to my family for their endless support in everything I do.

Author statement:

I declare that the presented work was developed independently and that I have listed all sources of information used within it in accordance with the methodical instructions for observing the ethical principles in the preparation of university theses.

Place, date	Signature

Abstract

Although ARDSnet is currently the preferred method of lung-protective ventilation, an individual positive end-expiratory pressure (PEEP) setting could mitigate the risk of lung injury. Following the ARDSnet guidelines, values of PEEP and FiO_2 are set based on oxygenation, regardless of the lung mechanics. Electrical impedance tomography (EIT) offers local ventilation assessment at the bedside. Interpretation of reconstructed EIT images is intuitive; comparison of regional effects across various PEEP steps is, however, difficult.

In this thesis, PEEP titration measurements of five porcine models with lavage-induced acute respiratory distress syndrome were analyzed. EIT-based local compliance values were used to derive features that enable easier quantification and description of regional compliance changes. Values of atelectasis, overdistension, center of gravity, and center of ventilation were calculated and used to evaluate ventilation performance across PEEP levels. Consequently, the features were combined using a fuzzy inference system and a set of rules to produce a single value that evaluates the ventilation from the perspective of local compliance.

The results showed that the ideal PEEP value considering the local compliance could be higher than the value suggested by global compliance. Furthermore, a high correlation was observed between global compliance and the sum of atelectasis and overdistension. That showed that this feature brings no added value unless evaluated separately.

The conclusions should be evaluated on a bigger dataset with finer PEEP steps. If the results are confirmed, a similar system could motivate the clinicians to use different PEEP values and facilitate the interpretation of EIT images.

Keywords: Electrical impedance tomography, Mechanical ventilation, PEEP, ARDS.

Abstrakt

Přestože ARDSnet je dnes preferovanou metodikou protektivní plicní ventilace, individuální nastavení hodnoty pozitivního tlaku na konci výdechu (PEEP) by mohlo omezit riziko poškození plic. ARDSnet stanovuje hodnoty PEEP a FiO_2 bez ohledu na mechaniku plic, pouze na základě oxygenace. Elektrická impedanční tomografie (EIT) umožňuje lokální posouzení kvality ventilace přímo u lůžka. Interpretace rekonstruovaných obrazů je intuitivní, avšak porovnání napříč změnami PEEP není snadné.

V této práci byla analyzována měření z PEEP titrací na pěti prasečích modelech s uměle navozeným ARDS. Z lokálních hodnot poddajnosti získané z EIT dat byly odvozeny charakteristiky, které umožňují snazší kvantifikaci a popis lokálních změn. Byly vypočteny hodnoty pro kolaps a nadměrné rozepnutí plic, těžiště a těžiště ventilace a na jejich základě ohodnocena kvalita ventilace napříč úrovněmi PEEP. Tyto charakteristiky byly dále zkombinovány ve fuzzy inferenční systému, a za použití jednoduchých pravidel byla odvozena jediná hodnota vyjadřující kvalitu ventilace z pohledu lokální poddajnosti.

Výsledky ukázaly, že ideální hodnota PEEP s ohledem na mechaniku plic by mohla být vyšší než hodnota odvozená na základě globální hodnoty poddajnosti. Dále byla prokázána vysoká míra korelace mezi globální hodnotou poddajnosti a součtem hodnot kolapsu a nadměrného rozepnutí. To ukazuje, že tato metrika neposkytuje přidanou hodnotu, pokud není posuzována odděleně.

Závěry by měly být ověřeny na větším datasetu s menšími kroky mezi hodnotami PEEP. Pokud se výsledky potvrdí, mohl by podobný systém motivovat lékaře ke zvážení jiných hodnot PEEP a usnadnit interpretaci EIT.

Klíčová slova: Elektrická impedanční tomografie, Umělá plicní ventilace, PEEP, ARDS.

Překlad názvu práce: Klasifikace změn poddajnosti dýchacího systému během mechanické plicní ventilace pomocí elektrické impedanční tomografie

Contents

Symbol List

Abbreviations

RWTH Aachen	Rheinisch-Westfälische Technische Hochschule Aachen
CTU Prague	Czech Technical University in Prague
O_2	Oxygen
CO_2	Carbon dioxide
FiO_2	Fraction of inspired oxygen
PaO_2	Partial pressure of oxygen in the arterial blood
PEEP	Positive end-expiratory pressure
EIT	Electrical impedance tomography
ARDS	Acute respiratory distress syndrome
MV	Mechanical ventilation
ICU	Intensive care unit
CoV	Center of ventilation
CoG	Center of gravity
FIS	Fuzzy inference system
MF	Membership function
VILI	Ventilator-induced lung injury

Physical quantities

t	Time	[s]
V_T	Tidal volume	[ml]
C	Compliance	[ml/cmH_2O]
$\dot{V}$	Gas flow	[ml/s]
P	Pressure	[cmH_2O]

Mathematical quantities

ϵ	Error function
R	Reconstruction matrix
$r(x, y)$	Pearson's linear correlation coefficient

1 Introduction

Mechanical ventilation (MV) is a widely used medical procedure. For patients with severe conditions, like acute respiratory distress syndrome (ARDS), MV is life-saving, as it facilitates the vital gas exchange. To secure the best ventilation performance and prevent harm to the patient, ventilator settings must be adjusted carefully. The recommended procedure is to follow the ARDSnet guidelines, which define several ventilation goals and correction procedures to maintain the goals.

The value of positive end-expiratory pressure (PEEP) is especially tough to select among ventilator settings while playing an essential role in the ventilation outcomes. Setting a PEEP that is too low may cause atelectasis, while choosing a PEEP that is too high may cause overdistention of the lungs. When the lungs are overdistended, the ventilator-induced lung injury (VILI) can quickly occur. VILI has several possible causes, of which the cyclic opening and closing of the alveoli is notable. In ARDS, the lungs are typically swollen, and the tissue's increased weight compresses the parts of the organ below. During inspiration, the ventilator creates a positive pressure to inflate the lungs, which opens the affected alveoli. However, during exhalation, these alveoli collapse again. Thus, an ideal balance between the two opposing phenomena has to be found. Finding the ideal PEEP value, leading to better ventilation performance, also enables reduced fraction of inspired oxygen (FiO_2) to be used, further decreasing the negative aspects of MV.

The ideal PEEP can be evaluated individually in a PEEP titration maneuver. However, global compliance is usually used to evaluate the PEEP value, which makes it challenging to monitor the underlying changes, as they can cancel out in the global parameters.

The ventilator settings can effectively change the lung mechanics of a patient. In particular, the global compliance is dependent on the current PEEP and tidal volume. Various local events cannot be observed or distinguished in the global parameter derived from the ventilation values due to oppositely acting changes in different regions. It is assumed that the local information could provide a better PEEP evaluation method concerning lung mechanics, minimizing the MV associated risks, and improving ventilation performance.

Regional compliance is calculated using electrical impedance tomography (EIT) images and reflects the compliance changes in a thorax cross-section. EIT offers affordable bedside lung monitoring, providing real-time regional insights into the lung function. While the regional differences in EIT can be observed intuitively in real-time, it is difficult to precisely compare the outcomes over time or after a PEEP change.

This thesis aims to analyze local compliance changes as extracted from the EIT measurements. To compare the global compliance changes with the local phenomena, a set of features based on the local data is designed. The purpose of the features is to quantify

the local changes in various ways. Finally, a fuzzy inference system is implemented, which combines all features, and using a set of rules, evaluates individual PEEP values.

The resulting evaluation provides a quick overview of the lung mechanics performance during the titration and might motivate the clinicians to consider slightly higher or lower PEEP levels than those suggested solely by global compliance value.

2 Theoretical background

In the following chapter, the theoretical background for the thesis is provided. First, the anatomy and physiology of the respiratory system and pathology of ARDS are introduced. It is necessary to understand the basics of respiratory system mechanics and the respective pathological processes to understand the difference and challenges arising when using MV in patients suffering from ARDS. Description of VILI follows, being one of the complications to avoid. Finally, the technical background of EIT, the primary source of data in this thesis, is provided, followed by a short introduction to fuzzy systems.

2.1 Respiratory system

The respiratory system (RS) serves multiple important purposes. First, it provides a supply of oxygen and lets off a waste product of cell metabolism, carbon dioxide. This process is referred to as the gas exchange. In addition, RS contributes to maintaining homeostasis and the immune system as a gateway for airborne pathogens.

The main organ of RS are the lungs. For purposes of this thesis, we can assume other parts of RS as passive airways only. Lungs provide gas exchange effectively owing to many alveoli, fine structures which increase the total effective area (to approximately 100 m^2 [1]). The function of the passive airways, besides of transport of the air to and from the lungs, is to filter, warm, and humidify the air going into the lungs.

2.1.1 Breathing mechanics

Under normal circumstances, breathing is facilitated by muscles of respiration, diaphragm, and intercostal muscles. The diaphragm separates the thoracic cavity and abdominal space. Intercostal muscles connect ribs, partly forming the chest wall. When the diaphragm contracts, it pulls the bottom of the thoracic cavity downwards. The external intercostal muscles pull the rib cage upwards, similarly to a scissor lift mechanism. Both activities contribute to the increase in the volume of the thoracic cavity. This creates negative pressure, which forces the lungs to expand as well, drawing air inside. During expiration, breathing muscles relax and return to the resting position, which takes approximately twice as long as the inspiration. The typical ratio of inspiration to expiration time (I:E ratio) is about 1:2.

Total lung capacity (TLC) in adults is over 6 litres. In terminology, this volume is divided based on anatomical or functional characteristics as depicted in Figure 2.1. Tidal volume (V_T) is the amount of gas expired at rest. Volume expired after a deep breath is called

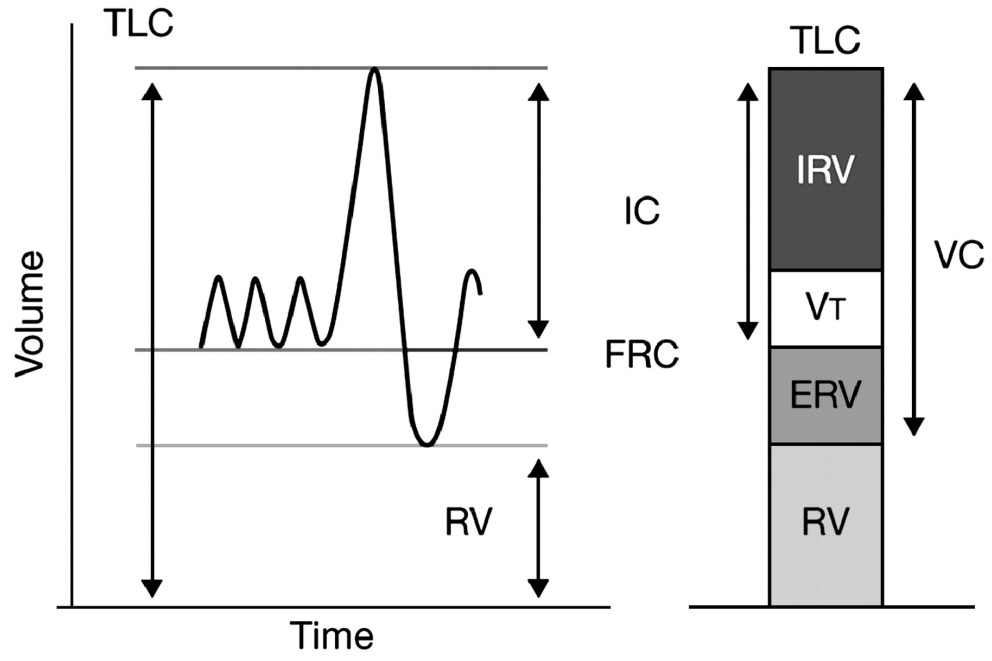

Figure 2.1: Volume values during gas exchange in lungs [2]. TLC = total lung capacity, IC = inspiratory capacity, VC = vital capacity, FRC = functional residual capacity, IRV = inspiratory reserve volume, V_T = tidal volume, ERV = expiratory reserve volume, RV = residual volume.

inspiratory capacity and is the sum of V_T and inspiratory reserve volume. The amount that can be actively expired in addition to normal expiration is called expiratory reserve volume.

Pressure changes during the breathing cycle similarly to the volume. Figure 2.2a shows the course of alveolar, pleural, and transpulmonary pressure (the pressure in alveoli, thoracic cavity, and difference of the previous two, respectively) during inspiration and expiration. Pleural pressure is always negative (-5 cmH_2O) and further decreases during inspiration due to the expansion of the thoracic cavity described above. Alveolar pressure, on the other hand, only slightly deflects from the ambient pressure (± 1 cmH_2O) as any change causes airflow. It can be also seen that the transpulmonary pressure is higher during active inspiration compared to passive expiration.

Figure 2.2b shows the pressure-volume loop of the lungs. It illustrates the hysteresis of the breathing cycle. The slope of the black dashed line represents the lung compliance. Lung compliance is a measure of lungs stiffness, or in other words its ability to stretch and expand. Typical value for a healthy adult is 200 ml/cmH_2O [3].

To model RS behavior, a simple RC circuit analogy can be used. As depicted in Figure 2.3, airway resistance (R in $cmH_2O/l/s$) and alveolar compliance (C in l/cmH_2O) are modeled as resistance and capacitance in a simple RC circuit. This model oversimplifies the complexity of lung mechanics but produces good estimations of RS parameters.

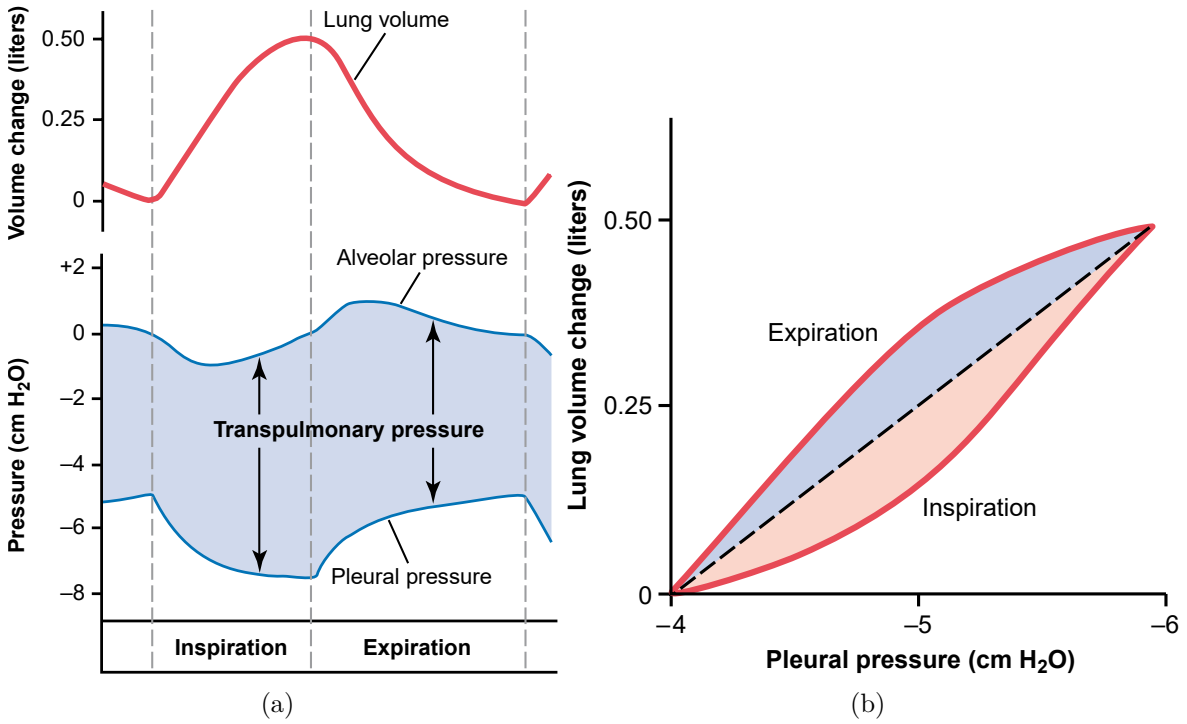

Figure 2.2: Respiratory system pressures. (a) Alveolar and pleural pressure during breathing cycle, (b) Pressure-volume curve visualizing lung compliance (black dashed line) [4].

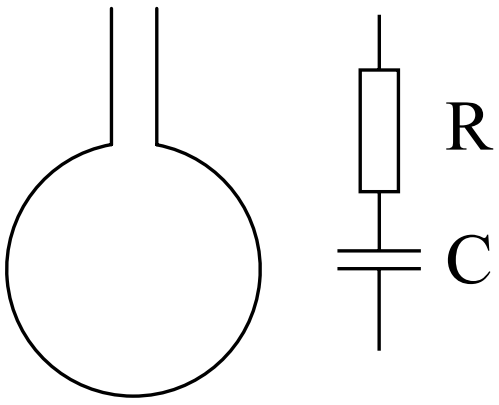

Figure 2.3: Equivalent electrical RC circuit model of lungs, adapted from [5].

Table 2.1: Partial pressures in respiratory system, values from [7] and [6].

	Pulmonary arterial blood	**Ambient air**	**Alveolar air, Pulmonary venous blood**
P_{O_2}	6 kPa	21 kPa	13 kPa
P_{CO_2}	6 kPa	0.04 kPa	5.3 kPa

2.1.2 Gas exchange

Gas exchange occurs at the blood-air barrier (also called alveolar-capillary membrane), which consists of an alveolar wall, basement membrane, and capillary wall. The membrane is very thin (2 μm), allowing gases to diffuse through it following the partial pressure gradients (Table 2.1) [6].

As FRC, the volume of air in the lungs at the end of expiration at rest is approximately four times greater than V_T, the alveolar air composition is different from ambient air because only part of it is exchanged for fresh air during each breath.

Alveolar wall also contains cells that produce surfactant (surface active agent), a substance that decreases surface tension, which helps keep the alveoli open and increasing the lung compliance.

2.2 Acute respiratory distress syndrome

ARDS was first described in 1967 by Ashbaugh et al. [8] on a group of 12 patients, characterized by acute onset of tachypnea, hypoxemia, and loss of compliance following various stimuli. The first definition of ARDS was published in 1994 by the American-European Consensus Conference [9] and the definition was updated in 2012 - the Berlin definition [10].

2.2.1 Definition

ARDS is defined by an acute onset - development of ARDS within 7 days of exposure to the risk factor. Risk factors include direct pulmonary injury (pneumonia, aspiration, contusion, smoke inhalation, pneumonitis, fluid embolus) and non-pulmonary conditions (sepsis, multiple trauma, pancreatitis, non-cardiogenic shock, drug overdose, transfusion-associated acute lung injury). If the risk factors are unknown, the cardiogenic origin of edema can be excluded using echocardiography.

Table 2.2: Degrees of ARDS severity with decisive PaO_2/FiO_2 ratio and respective mortality and ventilation days. PaO_2 is partial areterail oxygen level, FiO_2 is fraction of inspired oxygen.

ARDS Severity	**PaO_2/FiO_2**	**Mortality**	**Median duration of MV in survivors**
Mild	200 - 300	27 %	5 days
Moderate	100 - 200	32 %	7 days
Severe	<100	45 %	9 days

Bilateral infiltrates on chest imaging which cannot be explained by effusion, collapsed lung, or lung nodule is the imaging criterion of ARDS [11]. Figure 2.4 shows the first-week evolution of ARDS as seen on the chest radiograph.

X-ray is a cheap and widely available examination for fast identification, however, the patient is exposed to ionizing radiation. EIT (if available) could potentially replace x-ray in the image criteria.

The Berlin definition further specifies three mutually exclusive degrees of ARDS based on hypoxemia. Categories of ARDS are summarized in Table 2.2 alongside with respective mortality rates and the median duration of MV in survivors presented it the evaluation of the Berlin definition to illustrate the seriousness.

2.2.2 Baby lung concept

One of the signs of ARDS is the reduced size of the lungs caused by the edema. In most ARDS patients, the volume of normally aerated tissue is reduced to the size similar to the lungs of 5-6 years old child, and is therefore called "baby lung". Gas exchange primarily occurs in this area. It is, however, important to notice that the baby lung is a functional concept, rather than anatomical, and can shift depending on patient positioning.

If the edema is distributed throughout the whole lungs, it increases the hydrostatic pressure in the gravitationally dependent regions and pushes out most of the air as a consequence [13]. Figure 2.5 illustrates the superimposed pressure caused by the increased mass of the edematous lung tissue. The distribution of the inflammation, however, depends on the ARDS severity and the causing factor.

As a consequence, the overall compliance decreases and the lungs are prone to damage from MV. Higher PEEP values are needed to overcome the superimposed pressure in the dependent regions, which on the other hand might lead to overdistension in less influenced sections [14].

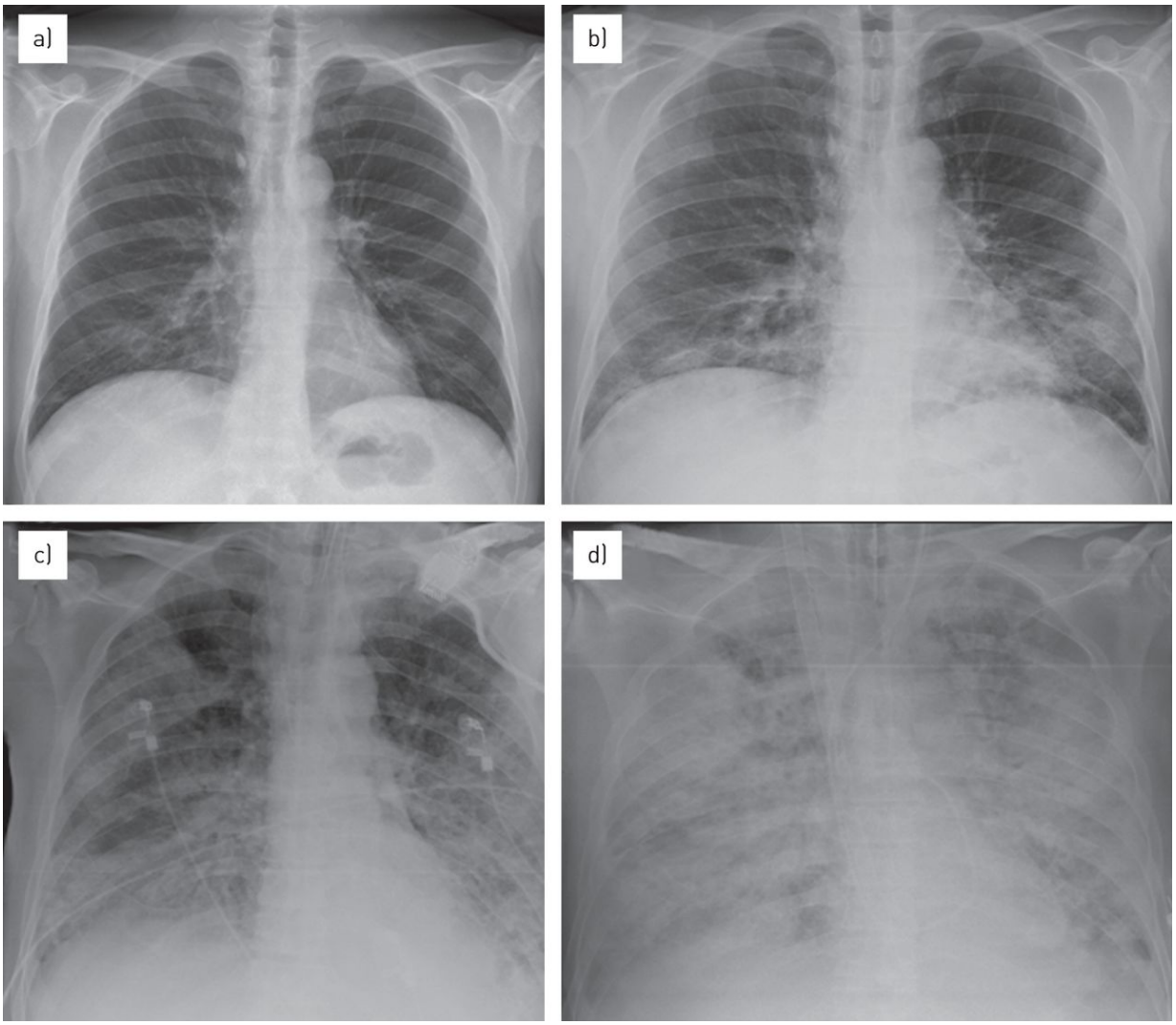

Figure 2.4: ARDS onset over the first week in a 57-year-old male with non-Hodgkin's lymphoma and H1N1 infection. a) Admission, no pathological findings. b) Second day, some pulmonary consolidations at the lower lobes. c, d) Next 2-3 days, a rapid deterioration of clinical and radiological conditions with consolidations (c) progressing to diffuse alveolar involvement, with "white lung" appearance (d) [12].

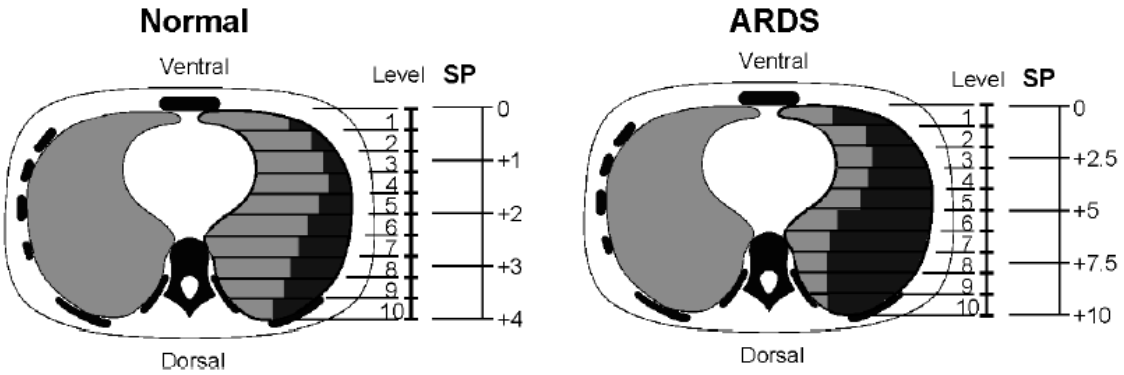

Figure 2.5: Comparison of normal and ARDS lung mass distribution. Increased superimposed pressure (SP, cmH_2O) leads to a collapse in the dependent regions [13].

2.2.3 Epidemiology

The incidence of ARDS shows significant variability over continents and countries. From South America with 10.1 per 100 000 person-years to the USA with almost 80 per 100 000 person-years. In Europe, the incidence is 17.9 per 100 000 person-years and ARDS makes up for 10 % of all ICU admissions. Despite the high incidence, up to 40 % of ARDS are not recognized by clinicians [15].

2.3 Mechanical ventilation

MV is a widely used medical procedure during which patients are intubated and connected to the ventilator. MV is utilized in planned surgeries to bridge the function of the lungs when the patient is sedated as well as intensive care units (ICU) to sustain life in critically ill patients.

The goal of MV is to supply oxygen and remove CO_2 as well as to monitor the function of the respiratory system. The ventilator supplements the function of breathing muscles, hence allowing patients to breathe even when sedated or in a coma. Therefore, MV is usually lifesaving, but at the same time, it is associated with serious complications. This is partly caused by the previous conditions of ventilated patients, who are usually at high risk of lung or cardiac compromise [16]. Complications of MV are described later in this chapter.

2.3.1 Working principle

Out of a variety of different MV types and approaches, only invasive positive pressure ventilation is relevant for this thesis. Invasive means that patients are intubated and therefore sedated. Positive pressure relates to the fact that the lungs are inflated by the positive pressure during the inspiration as opposed to the physiological breathing (or negative pressure ventilation, e.g. "iron lung", simulating this process).

Equation of motion of the RS (Equation 2.1) describes the relations of variables during the ventilation.

$$P_{\text{vent}} + P_{\text{musc}} = \frac{V_T}{C} + R_{\text{aw}} \cdot \dot{V} + \text{PEEP} + \text{PEEP}_{\text{i}} + I_{\text{aw}}, \tag{2.1}$$

where P_{vent} is the pressure provided by the ventilator, P_{musc} is the contribution of breathing muscles to the airway pressure, R_{aw} is the resistance of airways, $\dot{V}$ is flow, PEEP_{i} is intrinsic PEEP, which can be caused by an obstruction in airways and I_{aw} is the inertia of the gas flowing in airways.

For the calculations used in this thesis, the values of P_{musc}, PEEP_{i}, and I_{aw} can be neglected, and the Equation 2.1 can be simplified to the form

$$P_{\text{aw}} = \frac{V_T}{C} + R_{\text{aw}}\dot{V} + \text{PEEP} \tag{2.2}$$

This equation corresponds to the single compartment model of the lung introduced in Figure 2.3. Pressure, flow, and volume change continuously during the breathing cycle. Values of C and R are assumed to be constant (compliance changes with changes of PEEP as described later) and can therefore be derived by linear regression. The estimated values of C and R are reliable and physiologically meaningful when the P/V and $\text{P}/\dot{\text{V}}$ relationships are linear during the respiratory cycle [17].

The basic structure of the mechanical ventilator is schematically depicted in Figure 2.6a. Ventilators are designed to take compressed air and oxygen from wall outlets. The valves for both gases are electronically controlled to produce the desired pressure and fraction of oxygen. On the way towards the patient, air passes through the humidifier, as the parts of RS that would humidify the air under normal conditions are bypassed by the intubation. There is also an emergency shut-off valve. On the expiration side, pressure and gas flow are measured. The expiration valve allows the regulation of expiration flow and hence PEEP.

The user interface provides an overview of parameter settings and measured values and necessary controls to set and adjust ventilation mode, settings, and alarms.

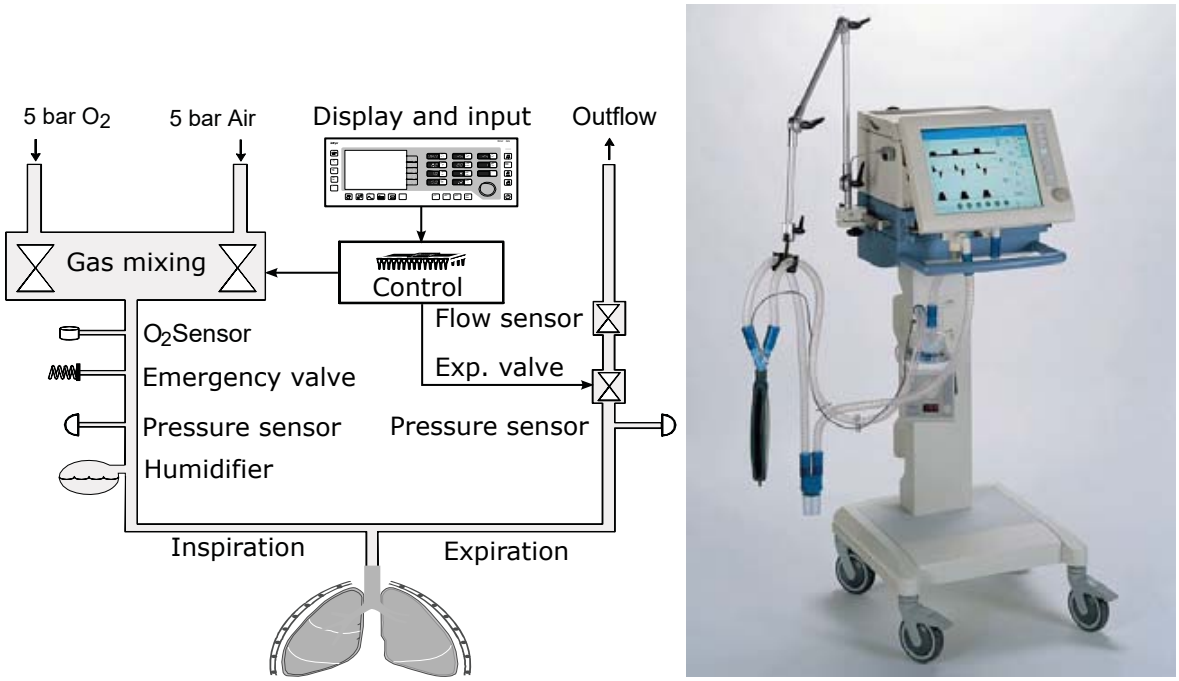

(a) (b)

Figure 2.6: (a) schema of components of mechanical ventilator, adapted from [18], (b) example of mechanical ventilator (Dräger Evita XL (2003)) [18].

The tubing is split into inspiration and expiration branch for the most part and only connects at the "Y" junction, which is right at the patient's mouth to reduce the dead space. The dead space is the volume of airways (naturally occurring anatomical and alveolar dead space) and tubing that has to be filled during each breath but does not contribute to the gas exchange.

Figure 2.6b shows an example of a complete ventilator (Dräger Evita XL (2003)), including the tubing set.

2.3.2 Ventilation modes

The operation of MV can be classified based on driving parameters of the breathing cycle. Assistive, patient-controlled modes are not relevant to this thesis. The two most common modes of ventilation are the Volume control (Volume-driven ventilation) and Pressure control (Pressure-driven ventilation) [19]. The typical course of pressure, flow, and volume during the breathing cycle are shown in Figure 2.7.

In Volume-controlled mode (also referred to as Continuous Mandatory Ventilation (CMV) or Intermittent Positive Pressure Ventilation (IPPV)) the desired tidal volume (V_T) and

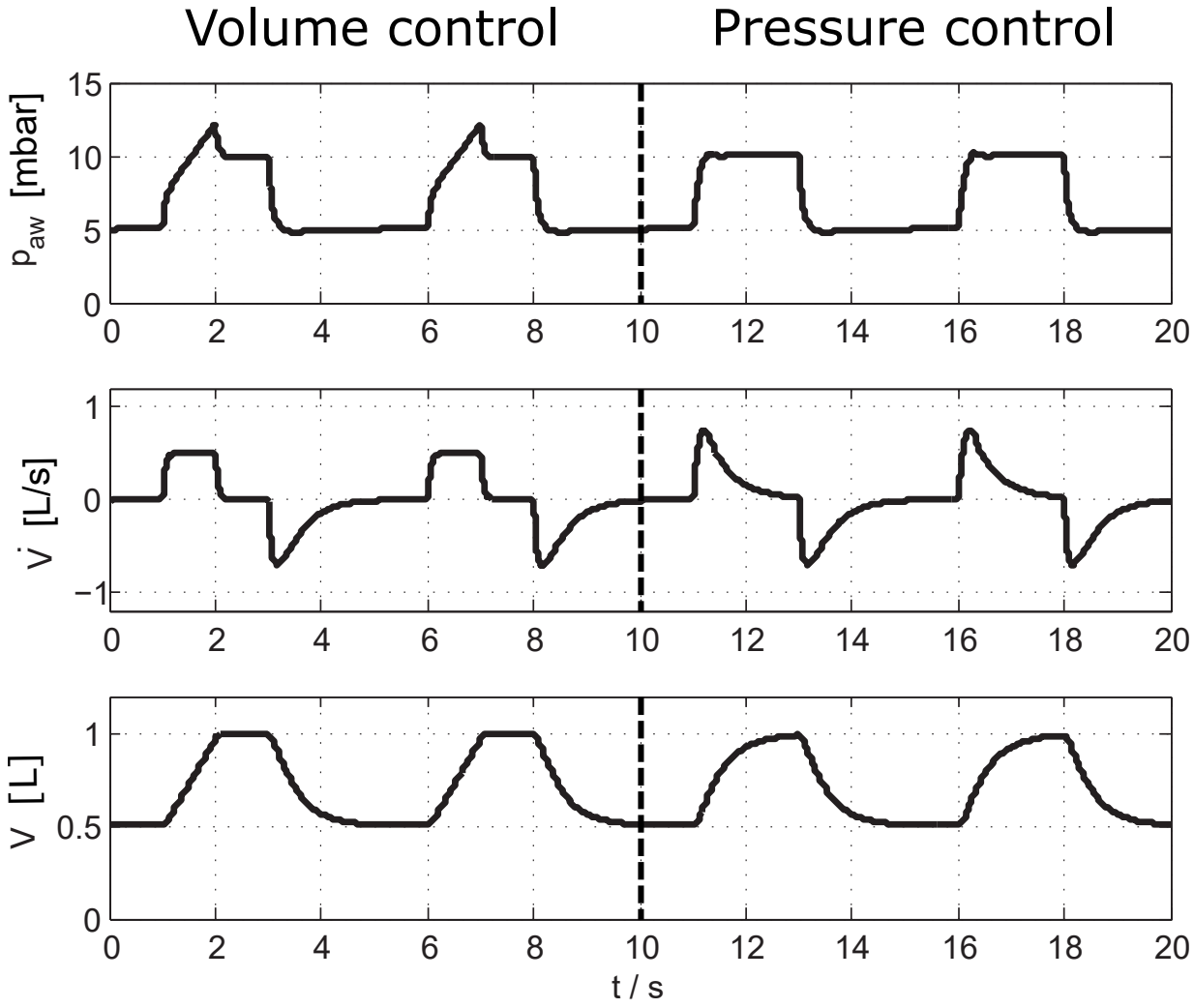

Figure 2.7: Volume-driven ventilation (left) and pressure-driven ventilation (right), adapted from [18].

inspiration time (derived from respiratory rate and I/E ratio) are set. The ventilator then delivers a constant flow required to achieve the V_T in a given time as can be seen on the left in Figure 2.7. Alternatively, the flow rate can be defined, in which case the ventilator derives the necessary inspiration time. The driving pressure is adjusted automatically to keep the flow rate and is dependent on the patient's lung compliance. Pressure driven ventilation In pressure-controlled mode the desired pressure is set and similarly to the volume control mode, inspiration time has to be defined. The ventilator delivers constant pressure, resulting in an initial peak in flow rate, followed by an exponential decrease as the lungs fill in as can be seen on the right in Figure 2.7. The resulting V_T achieved depends again on the patient's lung compliance. An increase in compliance leads to an increase in resulting V_T and vice versa.

In the dataset processed in this thesis, pressure-driven ventilation was used, with a driving pressure of 8 cmH_2O, respiratory rate of 25 breaths per minute, and I/E ratio of 1:1.

2.3.3 Parameters

Based on the mode of ventilation, some ventilation settings are kept constant and others are variable. Furthermore, a variety of parameters can be derived out of the measured values.

Driving pressure is the pressure produced by the ventilator. Usually defined in mbar or cmH_2O (often interchanged as 1 mbar = 1.02 cmH_2O), meaning that value of 0 is equal to the ambient pressure. The pressure difference (ΔP) is the difference in pressure at the end of inspiration and the end of expiration. Tidal volume is the amount of air delivered into the lungs during one breathing cycle. PEEP is the pressure that is superimposed over the driving pressure, keeping the lungs inflated during the expiration phase. This is achieved by restricting outflow with the expiratory valve. Intrinsic PEEP ($PEEP_i$) can be caused by high resistance, which leads to a cumulation of air inside the lungs (the next inspiration starts before the previous V_T is expired, see Airway flow in Figure 2.8 - at PEEP of 10 cmH_2O, there is the intrinsic PEEP). Inspiration to expiration ratio (I/E ratio) and the respiratory rate (RR) together define the length of inspiration and expiration. The fraction of inspired oxygen (FiO_2) is the fraction of oxygen in the inhaled gas. Natural FiO2 in the air is 0.21, which can be increased up to 1 (100 % oxygen) by adjusting the ratio of air and oxygen in the ventilator.

Compliance is a measure of the lungs' ability to expand. In absence of flow (at the end of inspiration and expiration), the equation of motion can be further simplified to $P = V/C$. By taking the difference between the end of inspiration and end of expiration, ΔP equals the driving pressure, and V_T the tidal volume achieved in case of pressure-controlled ventilation, or V_T equals preset volume and ΔP equals the pressure difference needed to achieve it in case of volume-controlled ventilation. Compliance can be then expressed as $C = V_T/\Delta P$.

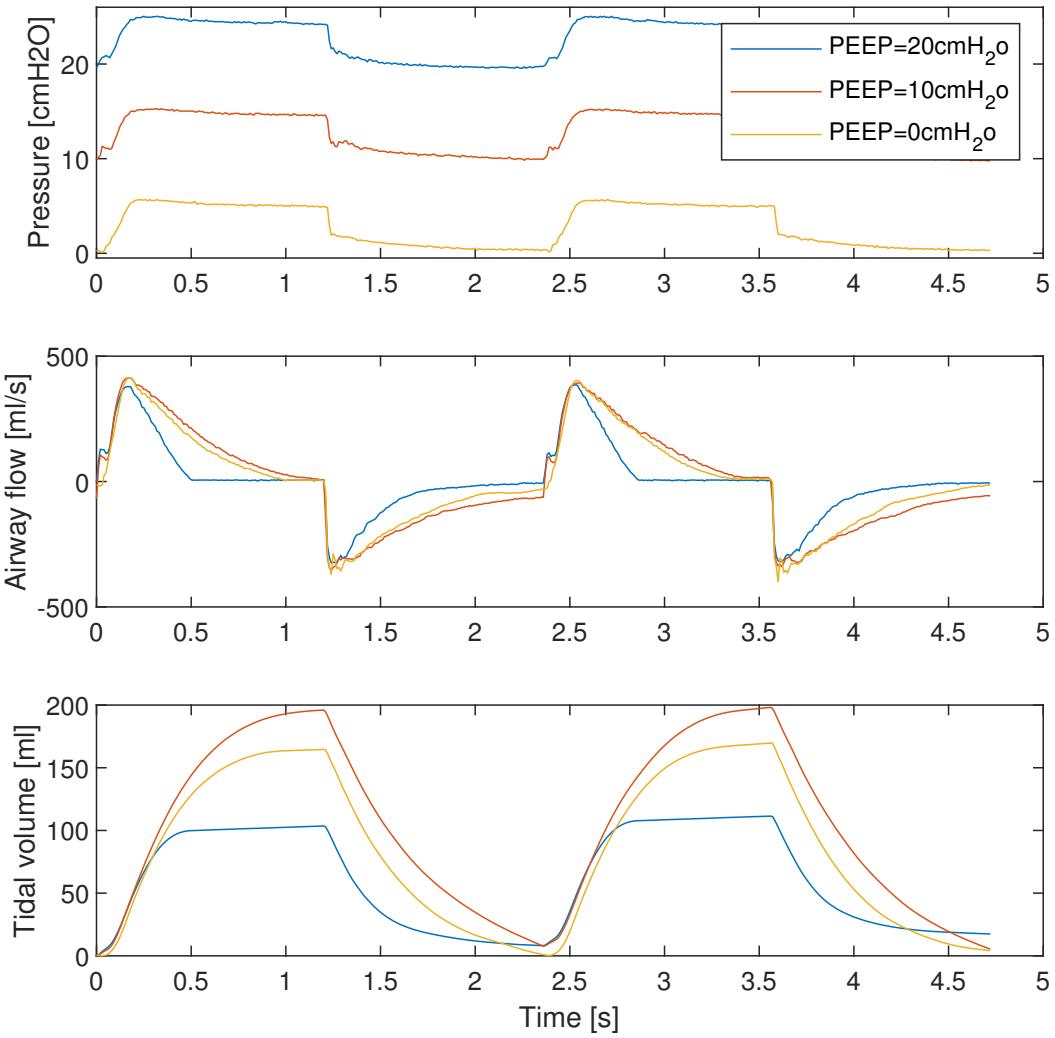

Figure 2.8: Comparison of airway pressure, flow rate, and volume values for different PEEP levels over two breathing cycles.

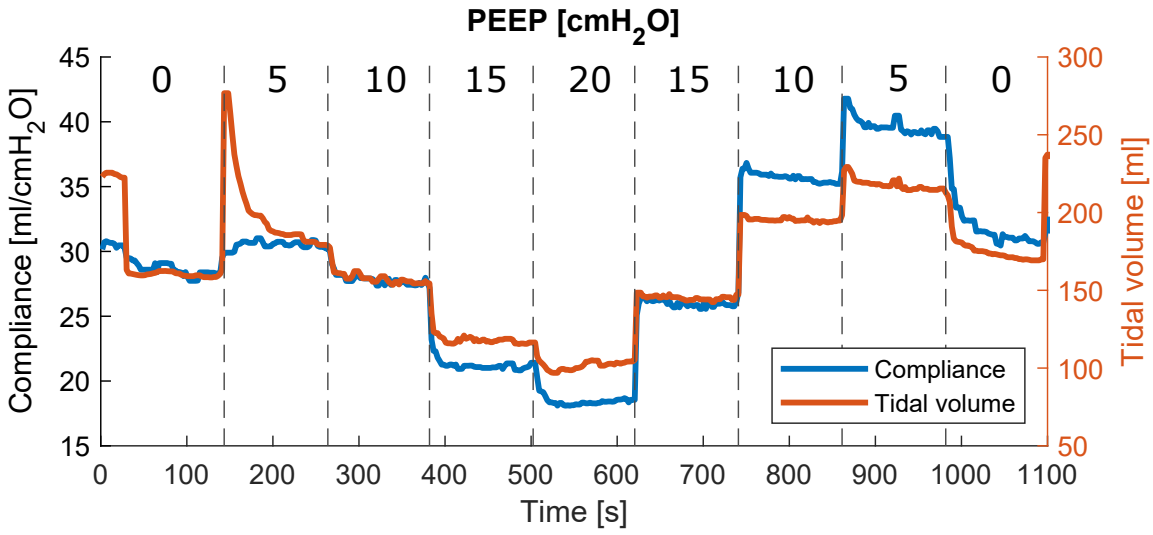

Figure 2.9: Course of compliance and tidal volume during the PEEP titration maneuver.

Figure 2.9 shows the course of compliance and tidal volume during the PEEP titration maneuver, where PEEP levels are increased and decreased in steps. Values of pressure, flow rate, and tidal volume for three PEEP segments (20, 15, and 10 cmH_2O from the descending section of PEEP titration) were shown in figure 2.8. The increase in compliance can be seen in the achieved tidal volume (values are correlated, as the driving pressure is constant), but also in the course of the flow rate. At the PEEP of 5 cmH_2O, the flow is present for almost the whole duration of inspiration as opposed to the previous values and it is higher (more negative) during the expiration.

2.4 Ventilator-induced lung injury

VILI is one of the potential complications of MV. It is one of the major concerns of the current MV development, balancing the clinical targets between benefits and potential risks to the patient. Patients with ARDS have a high probability of developing VILI, however, patients without ARDS are at risk as well [16].

2.4.1 Mechanics of VILI

Lung injury can manifest as a result of a variety of processes. Most important mechanics (volutrauma, atelectrauma, and biotrauma) are described below. Further effects on other organ systems (circulatory system, nervous system) are out of scope of this thesis.

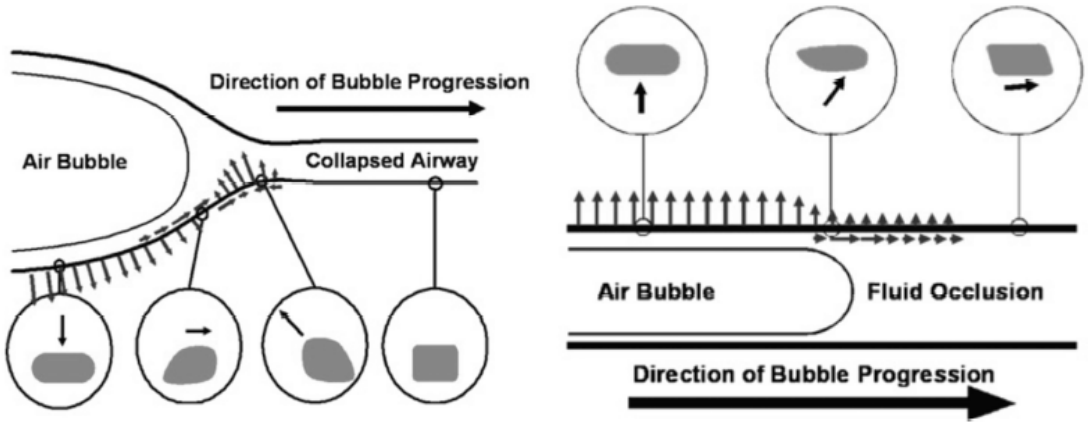

(a) (b)

Figure 2.10: Shear stress and strain during (a) opening of collapsed airway [22], and (b) propagation of air bubble along flooded airway [22].

Volutrauma is caused by over-inflation of the lungs, during which the tissue is damaged by the stretching [20]. Especially in less compliant lungs of ARDS patients, high V_T leads to overdistension of the relatively healthy alveoli, as they are more compliant than the affected ones. High airway pressure on its own does not cause VILI, as shown in the study by Dreyfuss et al. [21], which studied the influence of high volume and high pressure separately. Transpulmonary pressure, however, is related to the lung volume and therefore can affect the lungs similarly to high V_T [22].

Cyclic opening and closing of collapsed alveoli leads to atelectrauma. This is especially pronounced in ARDS patients due to the limited surfactant function and weight of the edematous lung tissue pressing the dependent lung regions. Figure 2.10 shows vectors of force caused by shear stress during the recruitment of collapsed alveoli. In case the alveoli are flooded, additional local stress at the interface between gas and liquid is created, which also leads to lung injury. [22]

If PEEP is set above the critical closing pressure of collapsed alveoli, they will stay open during the expiration, preventing atelectrauma. Alternatively, low tidal volume with low driving pressure could be used, leaving the collapsed parts closed during inspiration, utilizing only the more compliant regions of the lungs. EIT (described in more detail later) can provide useful insight and identify the collapsed regions of the lungs.

Biotrauma covers the biological response to the MV that can lead to activation of the inflammatory cascade, which may promote even to the lung regions not directly insulted by the MV. Furthermore, this can also lead to extrapulmonary organ injury, increasing the risk of multiorgan failure, hence the risk of death. [22]

2.4.2 Lung-protective ventilation

Lung-protective ventilation strategies represent different ways of preventing lung injury (i.e. VILI). Two major strategies are described below: ARDSnet and Open lung approach.

ARDSnet is a lung-protective strategy proposed by the ARDS network initiated by the National heart, lung, and blood institute (NHLBI)[1] with the aim to efficiently test promising agents, devices, or management strategies to improve the care of patients with ARDS. The guidelines provide initial ventilation settings and define 4 goals to lead the adjustment of the settings during the ventilation: oxygenation, plateau pressure, pH, and I:E ratio goal.

Predicted body weight (PBW) is used for V_T calculation. PBW is calculated according to equations 2.3 and 2.4 as

$$\text{PBW}_{\text{male}} = 50 + 0.91(h - 152.4), \text{ and} \tag{2.3}$$

$$\text{PBW}_{\text{female}} = 45.5 + 0.91(h - 152.4) \tag{2.4}$$

for men and women respectively, where h is the patient's height in cm. Ventilation is initiated with V_T of 8 ml/kg PBW, PEEP of 5 cm H_2O, and RR of less than 35 bpm. V_T is decreased by 1 ml/kg PBW in intervals shorter than 2 hours until it reaches 6 ml/kg PBW.

The oxygenation goal is guided by the FiO_2/PEEP tables. The goal is to keep PaO_2 55-80 mmHg or SpO_2 88-95 %. If the values are below the range, both FiO_2 and PEEP are to be increased according to the tables. The guidelines provide two tables for lower PEEP, higher FiO_2 (Table 2.3), and vice versa. Plateau pressure goal is maintained by tidal volume. If the plateau pressure exceeds 30 cmH_2O, V_T is decreased by 1 ml/kg, until the minimal value of 4 ml/kg. RR is adjusted to achieve the pH goal. If pH decreases below 7.3, RR is increased to up to 35 bpm, until pH >7.3, or $PaCO_2$ decreases below 25 mmHg. If pH further decreases below 7.15, V_T is increased in 1 ml/kg PBW steps until it returns. In case of increased pH (over 7.45), RR should be decreased if possible. Finally, the guidelines recommend that the duration of inspiration should be shorter or equal to the duration of expiration.

Furthermore, ARDSnet provides guidelines for patient weaning as well.

[1] http://www.ardsnet.org/files/ventilator_protocol_2008-07.pdf accessed on 04.01.2021

Table 2.3: Lower PEEP/higher FiO2 from ARDSnet oxygenation goal [23].

FiO_2	0.3	0.4	0.4	0.5	0.5	0.6	0.7	0.7	0.7	0.8	0.9	0.9	0.9	1.0
PEEP	5	5	8	8	10	10	10	12	14	14	14	16	18	18-24

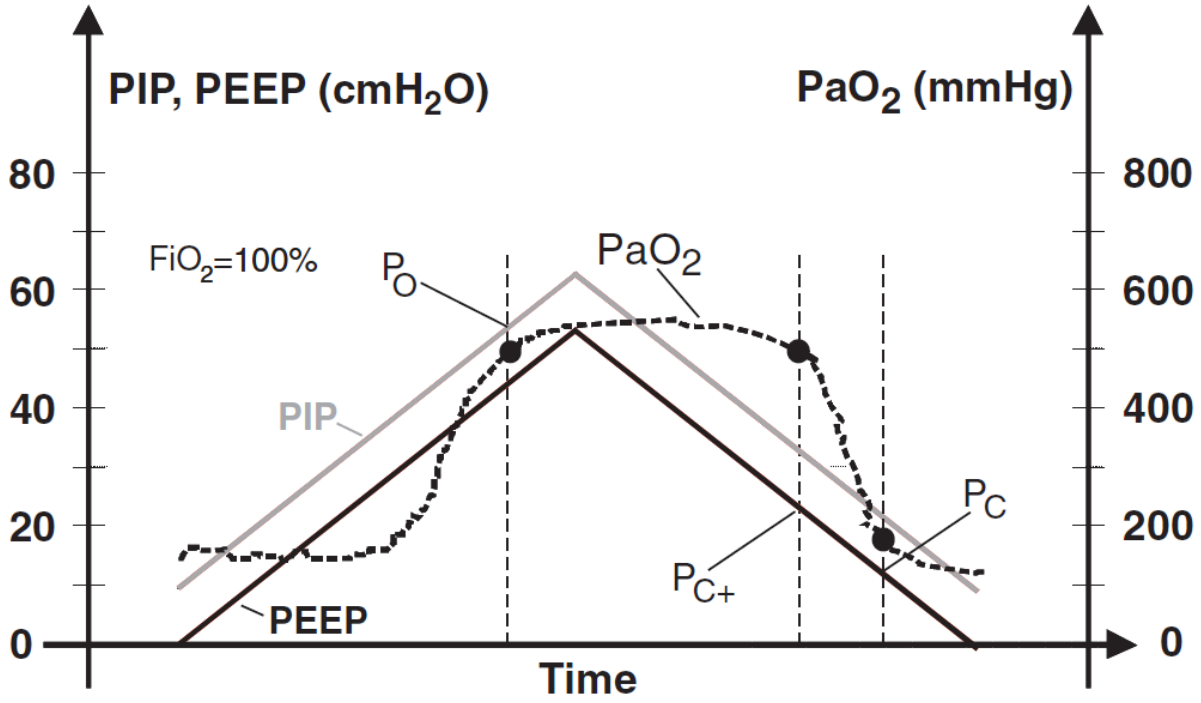

Figure 2.11: Identification of opening (P_O) and closing (P_C) pressure in PEEP titration based on PaO_2 [24].

The goal of the Open lung approach (OLA) is to identify the critical opening (P_O) and closing (P_C) pressure of the lungs in order to recruit the lungs and continue with ventilation at the lowest possible PEEP, thus preventing atelectrauma. Successful recruitment also maximizes PaO_2 and homogeneity of regional ventilation and perfusion. [24] Stepwise PEEP titration is used to find values of P_O and P_C. The lowest PEEP value that keeps the lungs open (P_{C+}) is then selected for the subsequent ventilation (Figure 2.11).

To compare the OLA and the ARDSNet protocol, a large, prospective, multicenter trial (ART)[25] that included 120 ICUs in nine different countries was conducted. In total, over 1000 patients were randomly divided between the OLA vs. the ARDSNet protocol of PEEP titration. Even though OLA has proven to be beneficial in terms of oxygenation without an increase in mortality in pilot studies [26], [27], the results of the ART study showed that 28-day mortality was significantly higher among patients treated with OLA compared to ARDSnet.

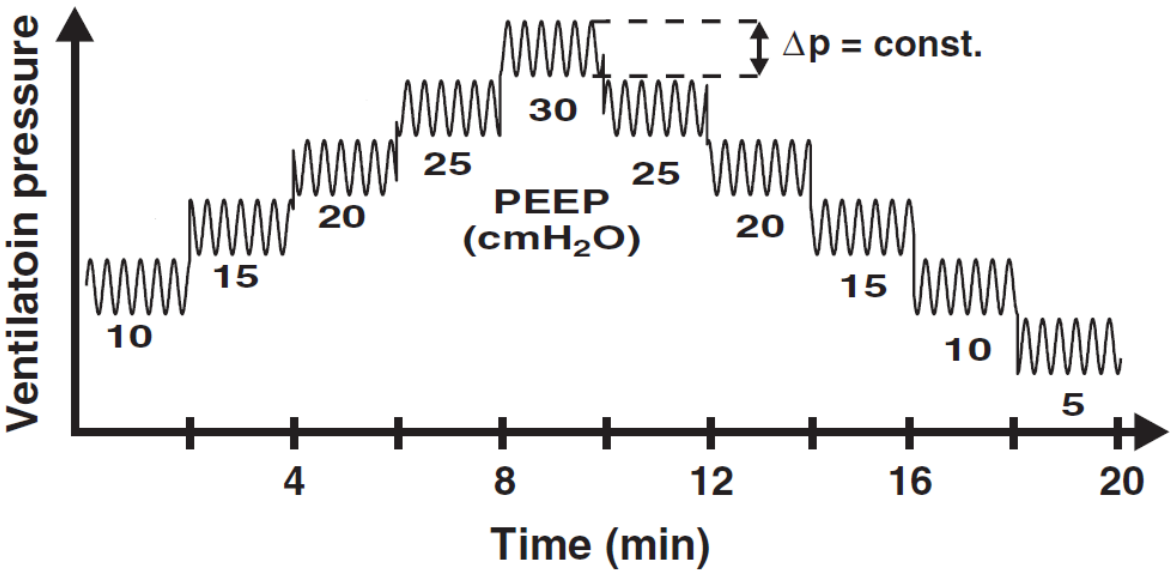

Figure 2.12: Course of pressure during the PEEP titration, adapted from [24].

2.4.3 PEEP titration

PEEP titration is a maneuver used to inspect the behavior of lungs in response to different PEEP values. PEEP levels are increased (and later decreased) in a given range by a constant value while monitoring patient data. Each step is kept for several minutes for the respiratory system to adjust to the new value. The typical course of ventilation pressure is shown in Figure 2.12. Alternatively, titration could start at high PEEP and only the decreasing section of titration would be performed.

Although the ARDSnet strategy, which does not utilize the PEEP titration, is de facto best practice today, PEEP titration can still provide individually tailored ventilation parameters. A clear disadvantage of PEEP titration is the time required to perform the maneuver, which requires a doctor's supervision. Nonetheless, automated PEEP titration protocols have been already proposed.

2.5 Electrical impedance tomography

EIT offers non-invasive, real-time monitoring of lung function. Although it cannot compete with computed tomography (CT) in terms of resolution and detail of regional lung condition, it can be easily used at the bedside for continuous monitoring and is radiation-

free. Furthermore, the time resolution of EIT measurements allows for the examination of the full breathing cycle, with current devices capable of framerate up to 50 Hz.

In this section, bioimpedance measurement is explained, and EIT device, measurement, data reconstruction, and interpretation are described.

2.5.1 Bioimpedance

Bioimpedance refers to the impedance of biological materials. It is the ability of the body or specific tissues to opposite the flow of electrical current, defined as a ratio of voltage (V) and current (I), as can be seen in Equation 2.5. To describe impedance in an alternating current (AC) circuit, we have to express it as a complex number as shown in Equation 2.6, where R is resistance and X_C is reactance, the opposition of the material to the change in the current flow [28]. As opposed to biopotentials, which are created by ion flow, bioimpedance is a passive electrical property.

$$Z = \frac{V}{I} \tag{2.5}$$

$$Z = R + jX_C \tag{2.6}$$

From the Equation 2.5, it is evident that the impedance can be measured using Ohm's law either by injecting known electric current and measuring voltage or vice versa, with the former being more common.

Lung tissue is well suited for the impedance measurement, as there is a significant change in conductivity during the breathing cycle. Although it might seem intuitive that the higher air volume at the end of inspiration acts as an insulator, the underlying effects are more complicated. Current pathways never pass through the air gap (considering medical device safety limits). Thus, they pass the same tissue, regardless of the air content, but the pathways might be longer, and the tissue characteristics change as the lungs fill.

Even though there are typical impedance values available from in-vitro measurements, the measurement of absolute EIT is challenging. Instead, differential EIT, which is independent of the absolute values, is the current state of the art. Method explanation is provided later.

2.5.2 EIT measurement

EIT measurement setup typically consists of a belt of 16 or 32 electrodes with one extra reference electrode and the EIT device itself. The device facilitates the current supply,

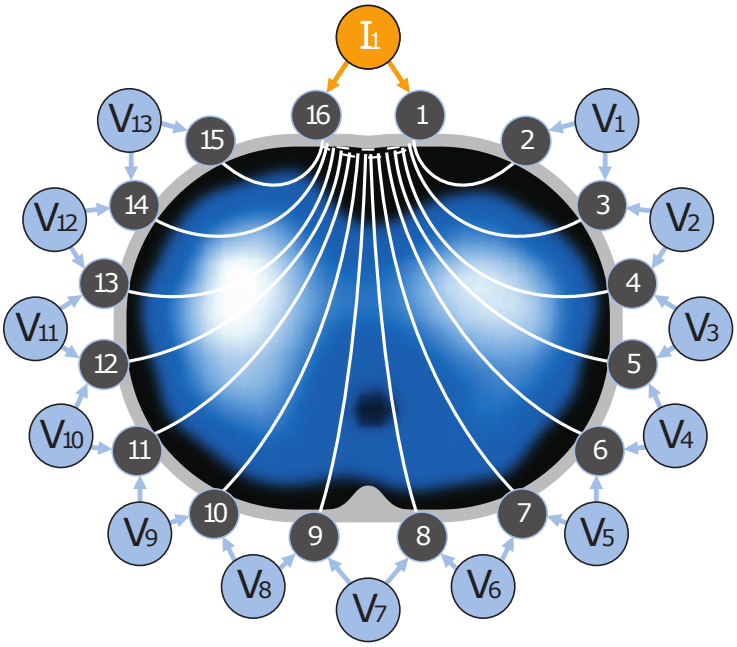

Figure 2.13: EIT current injection and voltage measurements, adjacent stimulation pattern [30].

multiplexer unit for selecting injection and measurement electrodes, voltage measurement unit, signal amplifiers, and the processing unit.

Although being challenged as ineffective [29], the adjacent stimulation pattern is still the most common measurement method. In the adjacent stimulation, a pair of electrodes is selected for the current injection, while voltage is measured between all neighboring pairs of remaining electrodes (Figure 2.13). The current injection pair selection is then shifted, and the next measurements are taken. The whole frame is completed once the injection pair rotates around the thorax [30]. Only half of the measurements are independent, as the same combination (injection, measurement) of pairs is used twice in each frame.

The measured data represent the impedance values measured between two neighboring electrodes for a given stimulation electrode pair. In the data available for this thesis, measurements were taken using 16 electrodes, resulting in 208 impedance values per one recorded frame.

2.5.3 Image reconstruction

In the next step, the images are reconstructed. Image reconstruction in EIT aims to calculate the impedance distribution in the measurement plane using the surface potentials as an input.

First, EIT prototypes used the same back-projection algorithm as CT scanners. The problem is that the current pathways are not straight nor parallel. Although back-projection can be used and produces images quickly, it suffers from inaccuracy, and low quality [31]. Gauss-Newton and GREIT are examples of more advanced reconstruction algorithms that are frequently used. In this thesis, the GREIT algorithm is used and therefore described in more detail below.

In 2009, Adler et al. introduced the Graz consensus Reconstruction algorithm for EIT (GREIT) [32]. GREIT is a linear reconstruction algorithm based on a 3D forward model. The algorithm produces a linear EIT image reconstruction matrix R. The image is reconstructed as

$$\hat{x} = Ry, \tag{2.7}$$

where $\hat{x}$ is the reconstructed image of dimensions $m \times n$, R is the reconstruction matrix, such that $R \in \mathbb{R}^{m \times n}$ and y are the input measurements [32].

Equation 2.7 looks very simple; however, the calculation of the reconstruction matrix R is complicated.

First, a forward model, which simulates the measurement, is created. For a given impedance distribution, surface potentials can be calculated for defined electrode pairs, given the injection electrode pair. The body cross-section is modeled with a finite number of nodes (finite element model, FEM). Later, targets of a known conductivity are inserted into the FEM to create a set of training data.

Subsequently, a noise model and performance metrics are created. The noise model accounts for electronic measurement noise and electrode movement artifacts.

Using the models and metrics described above, a set of training data is created, and the reconstruction matrix R is calculated such that it minimizes the reconstruction error ϵ^2 as

$$\epsilon^2 = \sum_k \|\tilde{x}^{(k)} - Ry^{(k)}\|^2_{W^{(k)}}, \tag{2.8}$$

where $\tilde{x}$ is the desired (simulated) image, W is a diagonal matrix of pixel weights, and k is the index of training measurements. The reconstruction matrix R then represents the best solution to the ill-posed inverse problem.

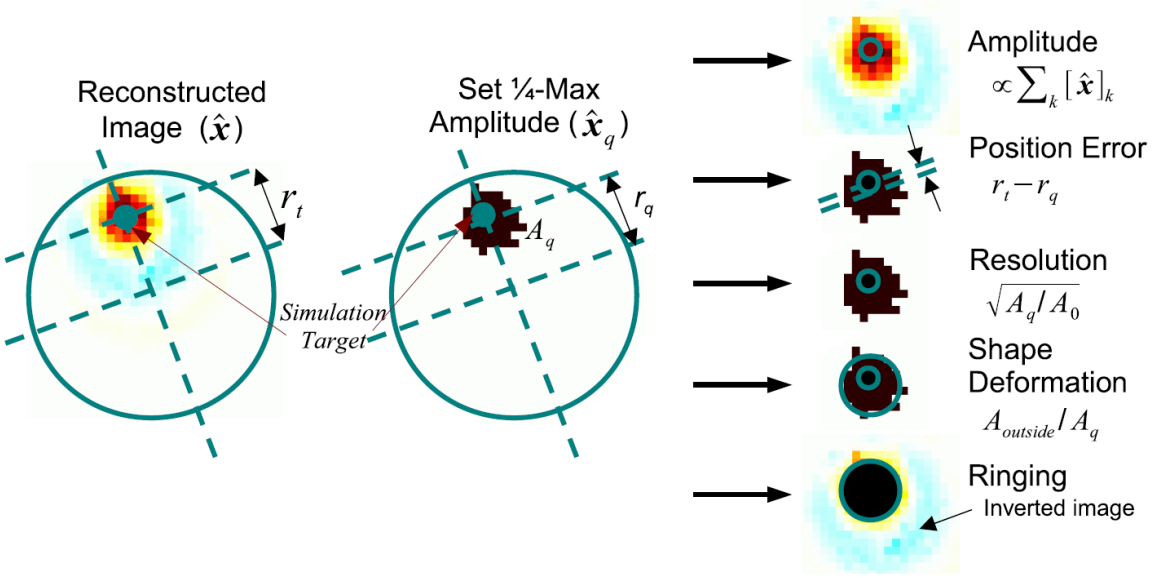

Figure 2.14: Figures of merit defined by Graz consensus Reconstruction algorithm for EIT [32].

Furthermore, the authors of GREIT define several figures of merit to evaluate the algorithm performance. The figures of merit are visualized in Figure 2.14 and briefly described in Table 2.4.

2.6 Fuzzy systems

Fuzzy sets, as defined by Zadeh [33] in 1965, is a logical framework that introduces logical operations for imprecisely defined classes. The motivation for this framework is that many classes outside mathematical definitions have ambiguous borders and smooth transitions with other classes. In the fuzzy set theory, objects do not have one class assigned, but rather a set of values representing a "grade of membership" in all defined classes.

In parallel to the "true" or "false" values of the Boolean logic, the fuzzy logic offers a more flexible "degree of truth" to evaluate a statement [34].

Fuzzy systems are well established in relatively simple control systems due to their effectiveness and implementation transparency. However, as the system's complexity rises, it becomes increasingly challenging to design or maintain the membership functions and rules. Therefore, fuzzy systems are often combined with neural networks in order to develop the system or to introduce the benefits of fuzzy logic to the neural network [34].

Table 2.4: Figures of merit for the evaluation of reconstruction algorithm [32].

Figure of merit	Equation	Description
Amplitude response	$\mathrm{AR} = \frac{\sum_k [\hat{x}_k]}{V_t \frac{\Delta\sigma}{\sigma_r}}$	The ratio of reconstructed image amplitude and the target volume V_t with conductivity σ_t. Under constant AR at any position, the volumes are expected to produce the same results regardless of the position.
Position error	$\mathrm{PE} = r_t - r_q$	Difference between the target and reconstructed object position. Small value and small variability are desired for the reliability of the results.
Resolution	$\mathrm{RES} = \sqrt{\frac{A_q}{A_0}}$	The ratio of the number of pixels A_q of the reconstructed target and the number of pixels of the entire reconstructed medium A_0. Uniform values are desired for the correct positioning of reconstructed objects.
Shape deformation	$\mathrm{SD} = \frac{\sum_{k \notin C} [\hat{x}_q]_k}{\sum_k [\hat{x}_q]_k}$	The ratio of the number of pixels outside of a circle C^a with the area as the reconstructed object. Low and uniform values are desired.
Ringing	$\mathrm{SD} = \frac{\sum_{k \notin C \& [\hat{x}]_k < 0} [\hat{x}]_k}{\sum_{k \in C} [\hat{x}_q]_k}$	The amount of amplitude with negative sign surrounding the reconstructed object compared to the amplitude inside the circle C^a.
Noise amplification	$\mathrm{NF} = \frac{\mathrm{E}[\mathrm{mean}\lvert\hat{x}_t\rvert]/\mathrm{E}[\mathrm{std}\lvert\hat{x}_n\rvert]}{\mathrm{E}[\mathrm{mean}\lvert y_t\rvert]/\mathrm{E}[\mathrm{std}\lvert y_n\rvert]}$	The ratio of input and output SNR in terms of amplitude. Low NF is desired; however, as there is a trade-off between NF and other figures of merit, a value of 0.5 is considered sufficient.

[a] C is a circle centered at the center of gravity of the reconstructed object with an area equivalent to pixel area of the reconstructed object.

In some situations, the fuzzy notation is of use even though the variables can be precisely quantified, but the system rules are easier to formulate in terms of fuzzy classes. Two partially overlapping fuzzy membership functions will, in turn, form a threshold, but the transition between the two classes will be smoother than the crisp step in case a value-defined threshold was used.

MATLAB Fuzzy Logic Toolbox was used to design a fuzzy inference system. The toolbox offers an extensive set of functions and a GUI fuzzy system designer. The toolbox's documentation covers all functions and provides several step-by-step guides.

3 Methods

In the following sections, the whole implementation part of the thesis is presented. The sections are divided systematically according to the processing workflow, as outlined in Figure 3.1. A brief dataset description is also provided.

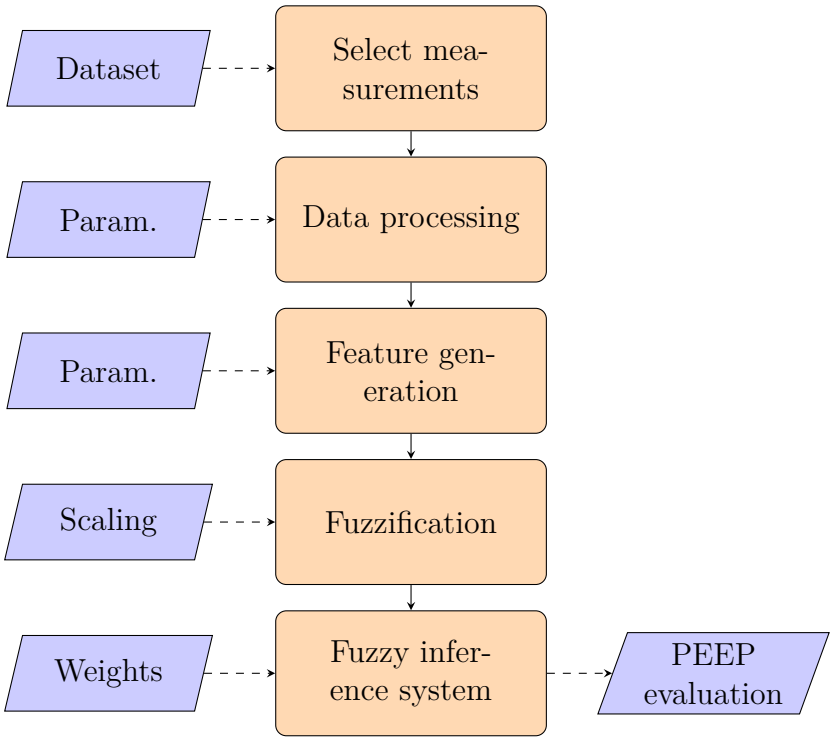

Figure 3.1: System overview. Orange blocks are the steps of processing workflow, blue trapezoids are inputs and outputs of the system.

3.1 Dateset description

The data used in this thesis were collected by Henning Luepschen in 2005. Part of the available dataset was previously published in [24].

A prototype EIT system (EIT evaluation KIT, Draeger Medical, Germany/GoeMF II system, University of Goettingen, Germany) was used to record a 16 electrode EIT measurement. Furthermore, a VentiLab setup consisting of a medically approved Panel PC (POC-153, Advantech Co., Ltd, Taiwan), an electrically controllable ventilator (Servo 300, Siemens-Elema, Sweden), an online blood gas monitor with a Paratrend 7+ sensor (TrendCare Satellite, Diametrics Medical Inc., USA), a hemodynamic monitor (Sirecust 1281, Siemens, Germany) and a capnograph (CO_2 SMO+, Respironics Inc., USA) was used.

In total, recordings for 14 pigs are available. The pigs were anesthetized, connected to the mechanical ventilator in a supine position, and the baseline measurement was taken. Subsequently, ARDS was induced by repetitive lung-lavage with warmed saline.

After a successful lavage, PEEP titrations were performed and recorded. Data from 13 measurement sessions were available, with one or multiple successful PEEP titrations per session. The dataset is summarized in Table A.2 in the Appendix. As the measurements took place over an extensive period, the naming conventions, and more importantly, the software versions changed. Therefore, sorting and preprocessing was necessary, as described below.

3.2 Data preprocessing

In this section, the steps preceding the automated data processing are described. The preprocessing mainly consists of manual tasks.

First, the corresponding pairs of EIT and ventilation measurements had to be matched in the dataset. The EIT and ventilation data were kept in separate folder structures, following the same pattern. However, the naming convention of the measurement files was not consistent in EIT and ventilation, nor among the individual measurements. There had been multiple recordings performed on each measurement day, hence each measurement contained up to three PEEP titration records and various baseline, lavage, and test recordings. Automated matching based on timestamps was not possible due to either bad synchronization of the measurement devices or later processing of the files.

For the reasons named above, a new dataset structure was created with manually selected measurement pairs of PEEP titration records. A tracking table linking the selected files to the original dataset was created in the process (see Table A.2 in Apendix). In total, 28 measurement pairs were selected.

As the measurements had taken place over a half-year time, the data format had changed. As a result, 11 measurement pairs from July 2005 were discarded because it was not possible to read the EIT data (header "Draeger EIT-Software V3.0") with an up-to-date EIDORS version. An effort was made to track down the version history of EIDORS, which was unsuccessful.

In subsequent visual inspection, the course of airway pressure and global impedance were displayed as well as a preview of few reconstructed EIT images from the beginning of the sequence. Two more records were discarded in this process - one record of a healthy subject (recorded before lavage) and one record with prematurely aborted downward PEEP titration. The validity of selected measurement pairs was checked based on measurement length, the number of PEEP steps, and steps' length.

Table 3.1: Parameters available in the ventilation data.

Parameter	Unit	Note
Airway flow	l/s	-
Airway pressure	cmH_2O	-
CO2 concentration	Volt	Unused, unknown reference
External flow	l/s	Unused
Relative lung volume	Volt	Unused, unknown reference
Trigger signal	binary	1 equals inspiration

3.3 Data processing

This section describes the processing of the EIT and ventilation data, calculation of derived parameters, and synchronization of the two data records.

The EIT data are loaded by EIDORS as measured impedance and stimulation pattern. Measured impedance is represented as a matrix where each column contains measurements for one frame in the order given by the stimulation pattern. As described in Theoretical background, the FEM approach is used to reconstruct the data, and therefore it has to be created first. Since all measurements processed in this thesis come from porcine models, a pig thorax geometry provided by EIDORS[1] was used. The GREIT algorithm was used to create the inverse model to reconstruct the EIT image data with a resolution of 64x64 pixels.

As described above, only part of the ventilation data was used. An overview of available parameters is given in Table 3.1.

The data were segmented into individual breathing cycles using the ventilator's trigger signal, and further parameters were derived for every breathing cycle, which are summarized in Table 3.2. Since the length of each breathing cycle is not constant, the first index of each breath was stored as a further parameter. Thereby, all cyclic parameters are assigned to an individual breath, which is related to the original ventilation data.

Steps in the PEEP signal were annotated automatically. First, the signal was filtered using a median filter to remove high-frequency fluctuations and keep the more significant steps. Positive and negative values of the first derivation of the PEEP signal correspond with increasing and decreasing steps, respectively. The absolute value of the first derivative was then used for peak detection. Since the titrations in the dataset usually end with several minutes of zero PEEP without any further steps, the last annotation is marked at the transition from PEEP of 5 cmH_2O to zero. As only segments before annotated steps are

[1] http://eidors3d.sourceforge.net/tutorial/GREIT/pig_ex.shtml accessed on 03.12.2020

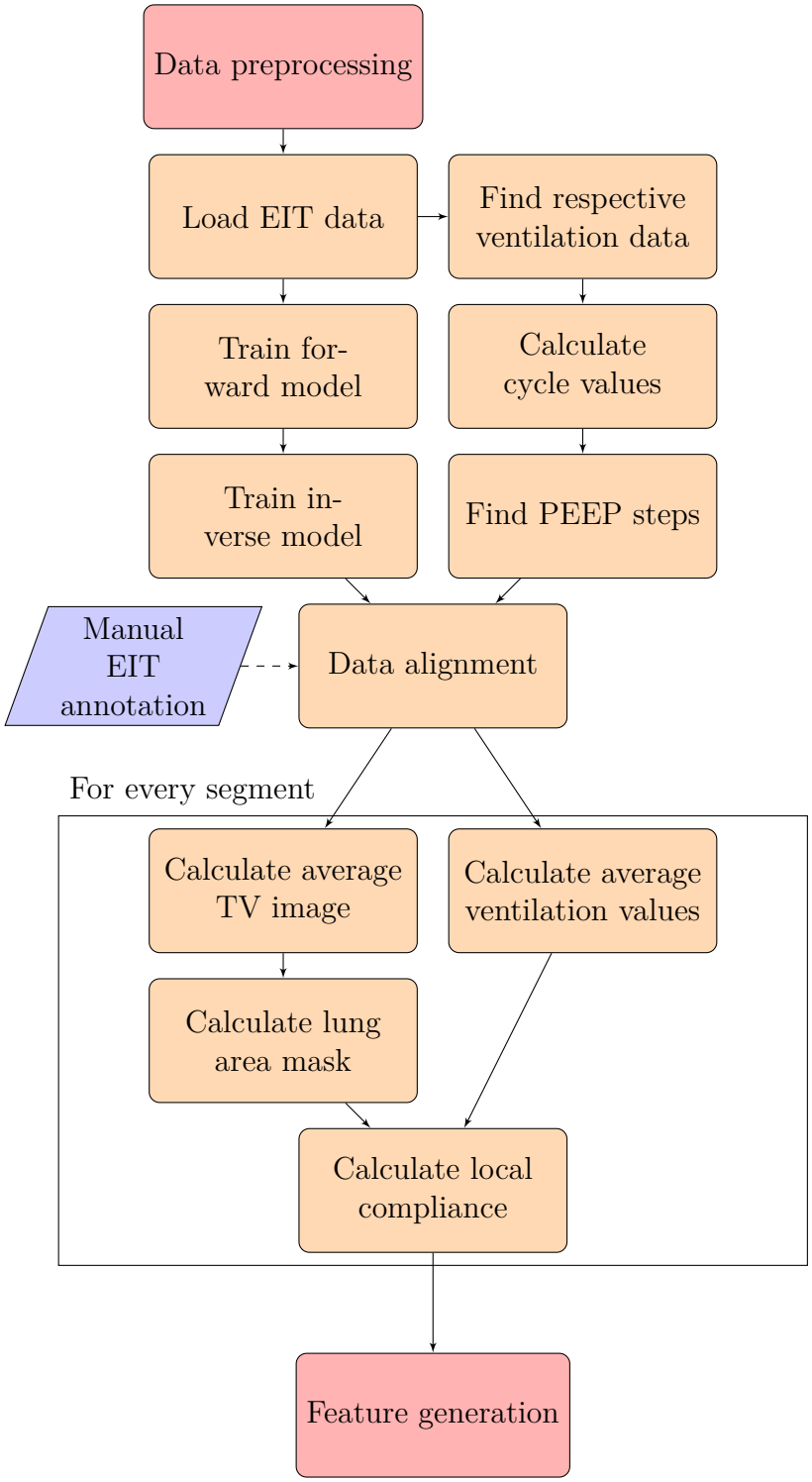

Figure 3.2: Data processing chain overview. Orange blocks are the steps of processing workflow, the blue trapezoid is user input, and the red blocks represent the preceding and following steps. The steps outlined by the rectangular frame are cyclically repeated for every PEEP level.

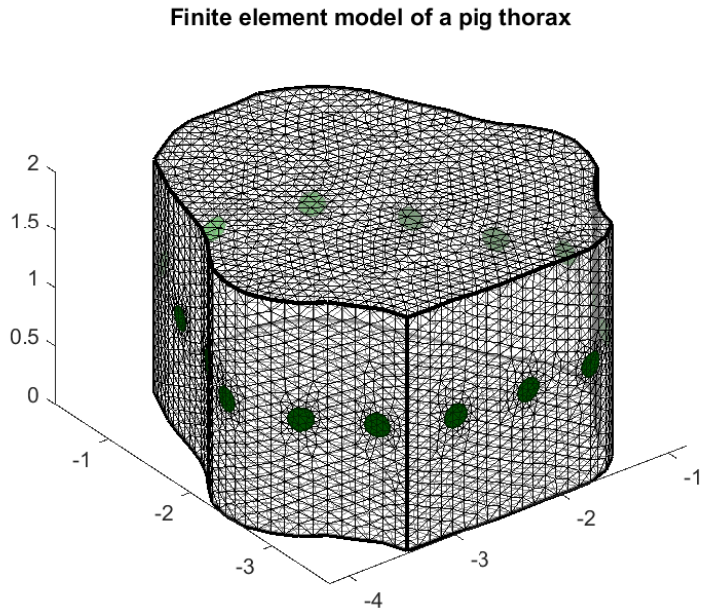

Figure 3.3: FEM of a pig thorax used to train the GREIT algorithm.

Table 3.2: Parameters of breathing cycle derived from ventilation data.

Parameter	**Symbol**	**Unit**	**Description**
Driving pressure	ΔP	cmH_2O	Calculated as a difference of minimal and maximal airway pressure in the breathing cycle
Positive End-Expiratory Pressure	PEEP	cmH_2O	Estimated as a minimal airway pressure in the breathing cycle. [a]
Tidal volume	V_T	ml	Airway flow is integrated to produce relative lung volume. The tidal volume is then calculated as a difference of minimal and maximal value.
Respiratory compliance	C	ml/cmH_2O	Calculated from tidal volume and driving pressure using equation of motion (Eq. 2.1) at assumption of zero flow (no airway resistance).

[a] For evaluation of individual PEEP levels during PEEP titration, average of the representative segment is taken and rounded.

considered in the processing, the last one would be missed. Therefore, two attempts are made to place one additional annotation at the end of the signal. First, at the average inter-step interval after the last one, and if the data are too short, at half the interval.

The global impedance trend tends to drift and has a longer response to the change of PEEP. Considering the small number of measurements available, a decision was made to annotate the PEEP steps in the EIT signal manually. For this purpose, a utility was made, displaying the PEEP signal from ventilation data with automatically annotated steps side-by-side with a global impedance signal (see Figure 3.4). The user is asked to mark the steps accordingly, and the values are stored. Next time the measurement is analyzed, the stored values are loaded (if available) and used, unless the number of steps differs from the number of steps recently generated for the ventilation data.

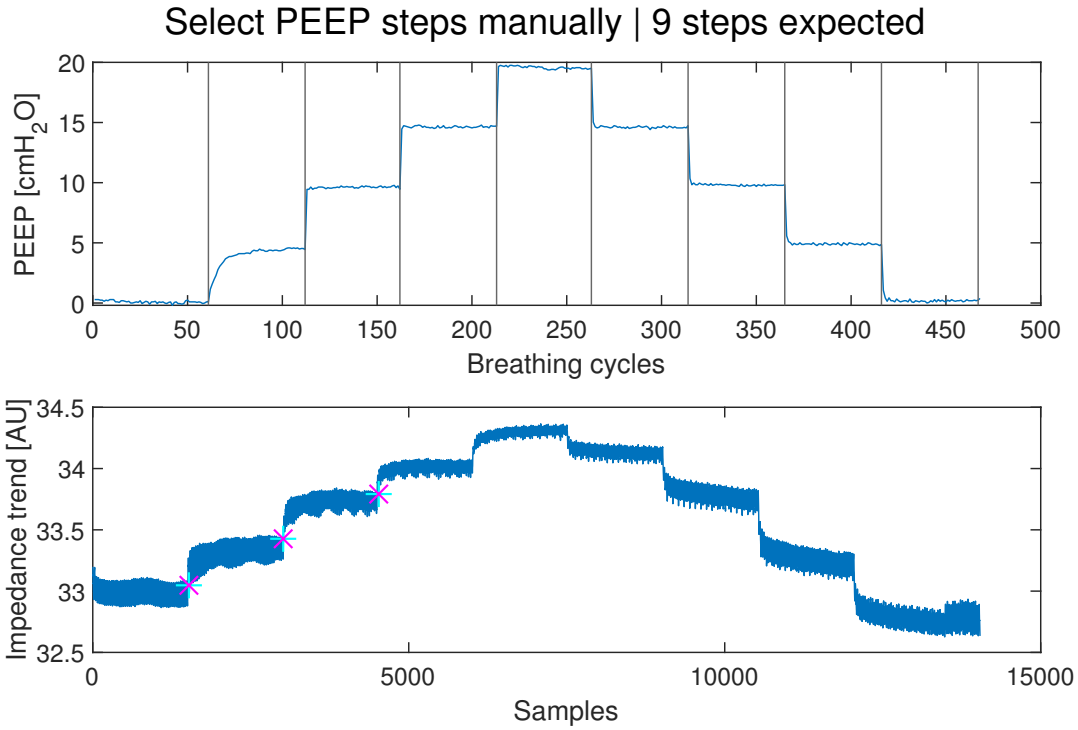

Figure 3.4: PEEP with automatically annotated steps (top) and global compliance (bottom). User is asked to manually annotate the steps in impedance signal. First three steps are marked here.

The sampling frequency differs for EIT and ventilation records. Furthermore, the start and end of the recordings were not synchronized, which means they can also vary in length and portion of the titration maneuver covered. Therefore, the data are synchronized using the PEEP step indices. The ventilation data record is used as a baseline and t=0 is set at the beginning of measurement. Best linear fit in a least-squares sense is found between the EIT and ventilation data step indices. Time vector for the EIT data is then derived relative to the ventilation data. Figure 3.5 shows an example of properly aligned data.

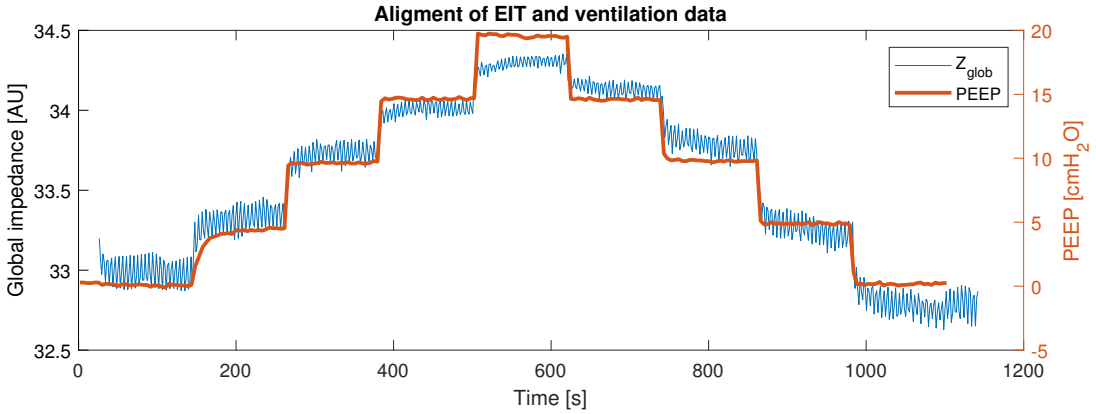

Figure 3.5: Aligned PEEP titration. Impedance data show slow response to change of PEEP, and drift (most noticable during the downward section of the titration). Tidal variation (the amplitude range) of the impedance data decreases with high PEEP.

It was not necessary to achieve perfect alignment, as subsequent evaluation of PEEP levels and feature generation was based on averaged values calculated on a representative segment for both EIT and ventilation data.

3.4 Feature generation

Before features were calculated, further processing for individual PEEP levels was necessary. This section explains all calculations performed for the individual PEEP step.

PEEP step annotations were used to prepare representative segments of the data for a given PEEP level. Segments were first examined for sufficient length to cover the desired segment duration and a margin. Segments that were too short were discarded. A 5-second margin was used to prevent the influence of the step change in case of imprecise annotation. Then 30-second segment preceding the PEEP step (taking the margin into account) was selected as shown in Figure 3.6. Indices for EIT measurements and cyclic ventilation parameters were taken from the samples best corresponding with the given time. Furthermore, any incomplete breathing cycles at the beginning or end of the representative segment were discarded.

Ventilation parameters were averaged for each representative segment. It was assumed that the values were stable during the whole segment, and averaging was aimed solely at noise reduction.

The average tidal variation image was calculated from the representative segment of the EIT data. This, similarly to the ventilation data, reduced the noise and additionally

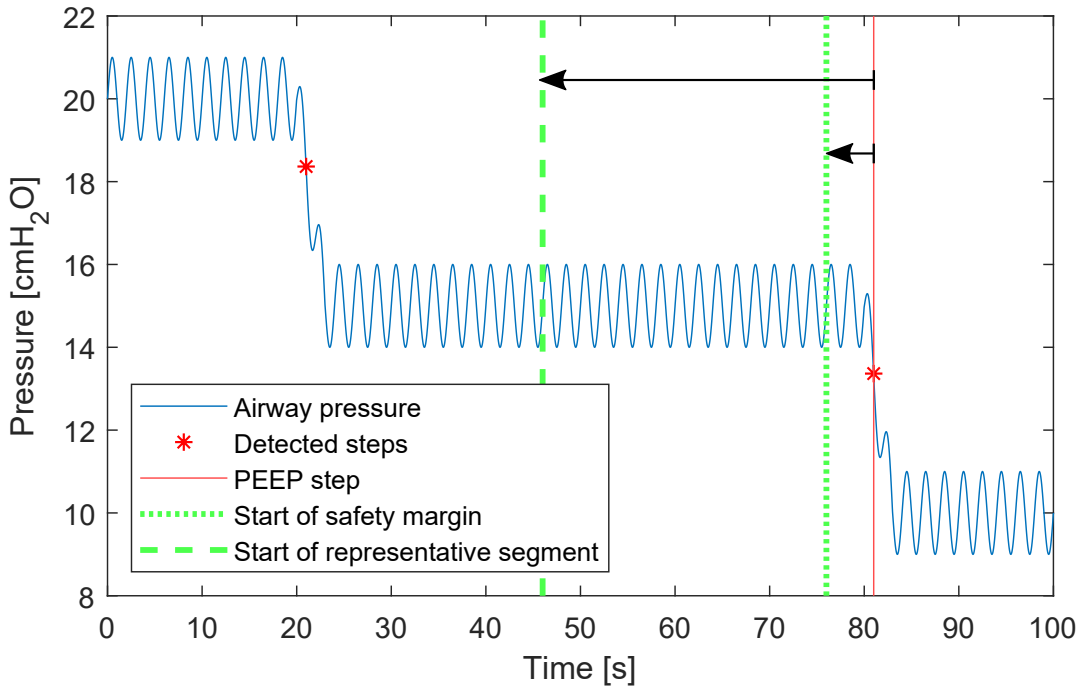

Figure 3.6: A representative segment and a safety margin are visualized on simulated PEEP steps. The safety margin prevents fluctuations close to the step in case the step is annotated imprecisely.

removed the influence of hearth beats, which are also captured in the EIT signal. For every breathing cycle in a given segment, the TV image was reconstructed from a difference of slices corresponding with maximal and minimal global impedance using the inverse model. Only the FEM coefficients were generated (not the 2D image pixel values) to prevent effects of value interpolation that takes place when getting pixel values based on the FEM. FEM coefficients are also stored in an array, and therefore easier to work with.

A lung area mask was created using a quarter amplitude set in order to limit the processed segment of the chest cross-section. The images had been processed without the mask at first. The border areas, however, had introduced unexpected behavior in the features. This was especially pronounced in the case of atelectasis and overdistension, as the implementation expects the compliance to follow the inverse "U" shape (described in detail later), which was not a general rule for the peripheral pixels. Therefore, the lung mask is used for all feature calculations.

Among other things, the quarter amplitude set is used by the GREIT algorithm to evaluate a reconstructed image [32]. It is a common practice in EIT processing and provides better results than thresholding of standard deviation of a pixel during the course of the representative segment that was implemented before.

Only pixels with a value greater or equal to the quarter of the value range of a given TV image were included in the mask, as described by Equation 3.1 [32]:

$$[x_q]_i = \begin{cases} 1 & \text{if} [x]_i \geq [\min(x) + \frac{1}{4}[\max(x) - \min(x)]] \\ 0 & \text{otherwise,} \end{cases} \tag{3.1}$$

where x_q is the mask and x the TV image.

Masks for all PEEP levels were afterward averaged, and only pixels present in half of the masks or more (average value >= 0.5, assuming binary mask, where 1 equals included, and 0 equals excluded) were included in the final mask. The same mask was then used to outline lungs at all PEEP levels of a titration. That enabled a comparison of values between individual levels.

The average TV image was then masked with the final mask and served as a basis for further processing. Images were first normalized so that the sum of all pixels was equal to 1 (the value of every pixel denotes its contribution to the image).

$$x_{\text{norm}} = \frac{x}{\sum x} \tag{3.2}$$

where x denotes pixels of masked TV image.

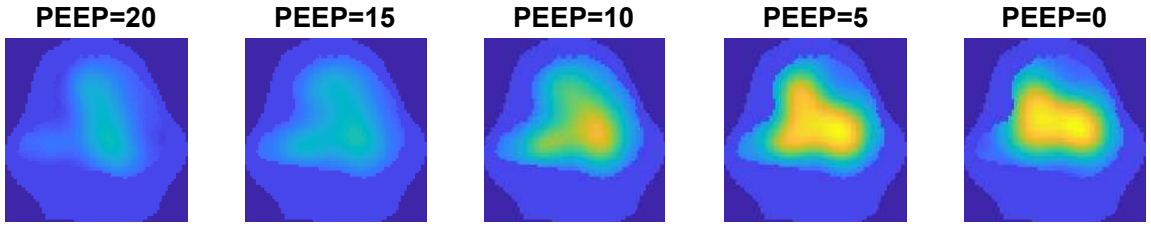

Figure 3.7: Tidal variation images masked with the final averaged mask built from quarter amplitude set mask of individual steps.

Next, values were multiplied by the V_T from the ventilation data. The resulting image represents the local distribution of tidal volume.

$$x_{\text{vol}} = x_{\text{norm}} \cdot V_T \tag{3.3}$$

where V_T is the tidal volume.

The local tidal volume image's pixel values were then divided by the driving pressure from the ventilation data, resulting in the local compliance image.

$$x_{\text{comp}} = \frac{x_{\text{vol}}}{\Delta p} \tag{3.4}$$

where Δp is the driving pressure.

The local compliance image is then used in all feature calculations. Furthermore, for the evaluation of compliance gain and loss, differential TV images were derived as a pixel-wise difference of compliance images at two consequent PEEP levels.

3.4.1 Center of gravity and ventilation

Images were first divided into four RIOs - bands of equal width stacked in a dorsal-to-ventral direction. Values of regional compliance were summed in each band for every PEEP level. To accommodate for an unequal number of lung pixels in each ROI, values were divided by the number of pixels, resulting in mean regional compliance of the ROI (see Figure 3.8).

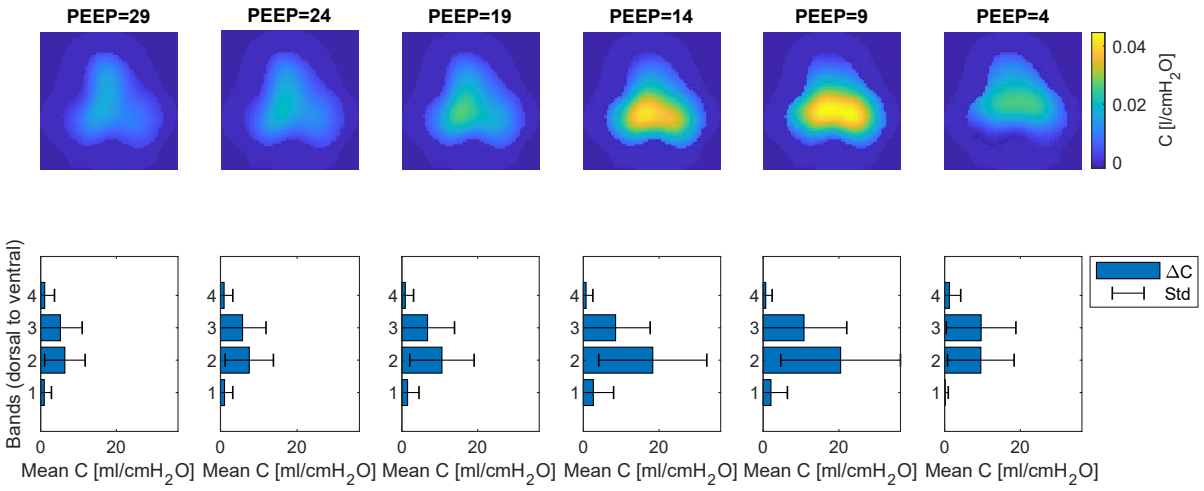

Figure 3.8: Mean regional compliance in four ROI. Increase in central regions is obvious. Furthermore, slightly higher values for the dorsal region can be observed at PEEP 14 and 9, with steep drop at lower level, while the value in ventral region decreases at those PEEP levels.

The compliance bands provided information about regional changes in compliance during the PEEP titration. Increasing the resolution to individual rows and abandoning the idea of averaging the compliance, the basis for the calculation of the center of gravity is created. In contrast with general interpretation of this term, the center of gravity in this context is only defined in one dimension - the dorsal-to-ventral axis (sometimes referred to as $\mathrm{CoG_y}$, notation of CoG and CoV is used for one-dimensional centers in this thesis).

Values for the center of gravity were calculated according to the definition by Luepschen et al. [24] as: eq where N is the resolution (same in both directions), x,y are the image coordinates, and F(x,y) are the pixel values of a regional compliance image. Consequently, the feature was extended with the definition of center of ventilation by Sobota et al. [35]. CoV aims to divide the row sum histogram into two equal halves. The normalized tidal variation image was used for the calculation (image sums to 1). First, the last row for which the cumulative sum of rows is less than 50% of the total is found:

$$n = \underset{i \in \mathbb{N}}{\operatorname{argmax}}(r_{\mathrm{cumsum},i} \leq 0.5) \tag{3.5}$$

where $r_{\mathrm{cumsum},i} = \sum_{j=1}^{i} r_j$ is the cumulative sum of row sums. Next, ratio k, which expresses the ratio of r_n according to the residual up to 50%, is calculated as:

$$k = \frac{0.5 - r_{\mathrm{cumsum},i}}{r_n} \tag{3.6}$$

Finally, the value of CoV is calculated as:

$$\mathrm{CoV} = \frac{n + k + 0.5}{N + 1} \tag{3.7}$$

The center of gravity (ventilation) produces a single value representing the coordinate that balances the image according to either definition. The values were converted to percent from dorsal-most to ventral-most coordinate.

Figure 3.9 shows CoG and CoV values that were calculated for TV images at every PEEP level, displayed over the row sum histogram.

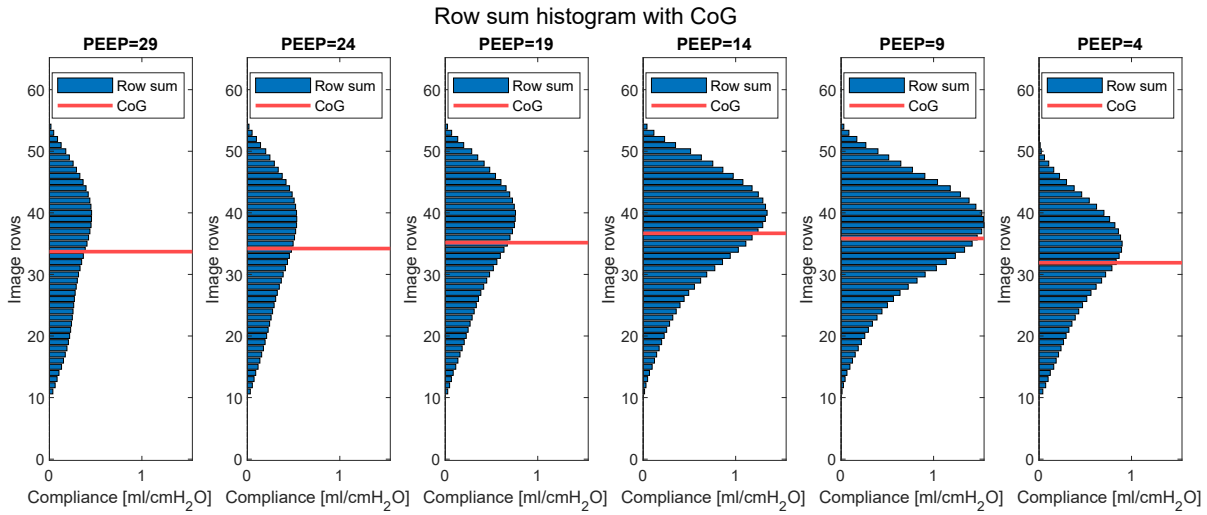

Figure 3.9: Histogram of row sums of regional compliance image with the center of gravity for various PEEP levels.

3.4.2 Atelectasis and overdistension

The concept of atelectasis and overdistension has a sound physiological rationale. Because of superimposed pressure caused by the weight of edematous lung tissue (see ARDS), the pressure needed to recruit alveoli differs depending on the region's position. For a given driving pressure, some sections may still be collapsed, while alveoli in other lung regions may suffer from overdistension.

Calculation of atelectasis and overdistension Following the method of Zhao et al. [36], pixels were classified as overdistended before reaching the maximal compliance, and analogically collapsed after this point. The highest compliance value was therefore found for each pixel, along with the respective PEEP level. A histogram of the number of pixels

exhibiting the best compliance value at a given PEEP level (see Figure 3.10) provides a first hint on the shape of atelectasis and overdistension curves. Pixels were subsequently classified, and the count of collapsed and overdistended pixels was calculated at each level. The values were then converted to percent of the total lung area.

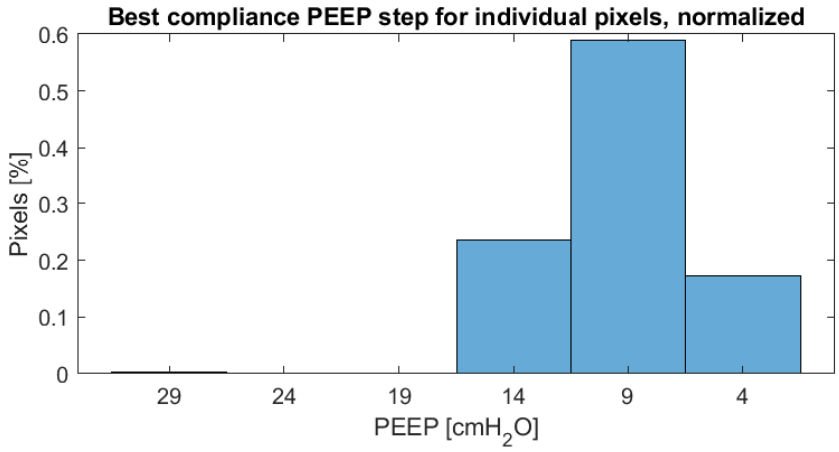

Figure 3.10: Number of pixels that show the best compliance values for a given PEEP level.

Figure 3.11 shows downward section of a PEEP titration with overdistension and atelectasis percentages for every level. Green line marks the level with the lowest sum of non-ideally ventilated pixels.

The thesis's documentation contains animated figures (gif) and scripts to generate them, which better visualize the changes in the course of PEEP titration. A single slice from this sequence can be seen in Figure 3.12.

Furthermore, a percentage-based method for atelectasis and overdistension was implemented, as defined by Costa et al. [37]. This method also considered how close the current pixel value was to the best one, therefore did not only classify the pixels as atelectatic or overdistended but quantified the effect.

The second method was also based on the local compliance values from tidal variation EIT image. For each pixel, the highest compliance values over the titration steps were found. The pixel was classified as overdistended at steps preceding the highest value step and analogically as collapsed after passing it. The atelectasis values were defined as:

$$\text{Collapse}_{\text{pixel}}\,(\%) = \frac{(\text{C}_{\text{best},p} - \text{C}_p) \times 100}{\text{C}_{\text{best},p}}, \tag{3.8}$$

where $\text{C}_{\text{best},p}$ is the highest compliance value, the pixel p exhibits over the course of the PEEP titration, and C_p is compliance value of pixel p at current PEEP. The value of atelectasis is set to 0 if the pixel has not yet reached the best compliance.

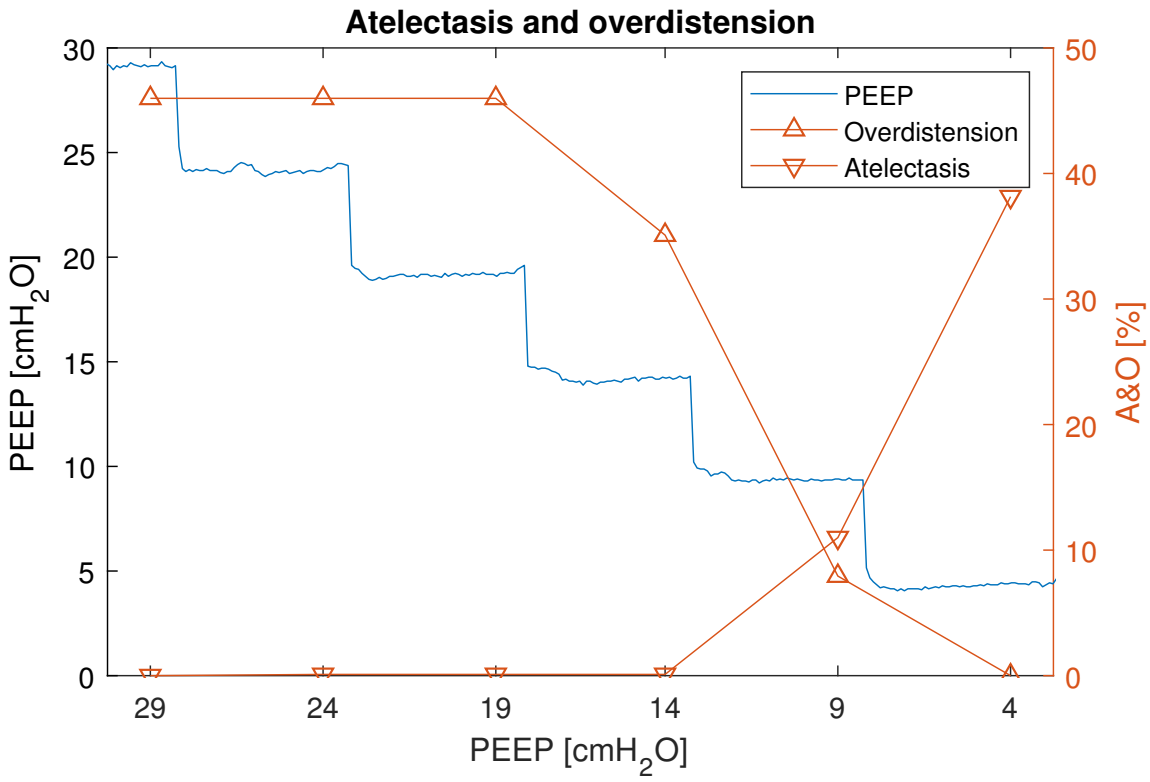

Figure 3.11: PEEP titration with corresponding atelectasis and overdistension (pixel-based) values. The need for finer resolution of PEEP steps is evident, as only one step (10 cmH_2O) is acceptable, while a slightly higher value might be a better compromise.

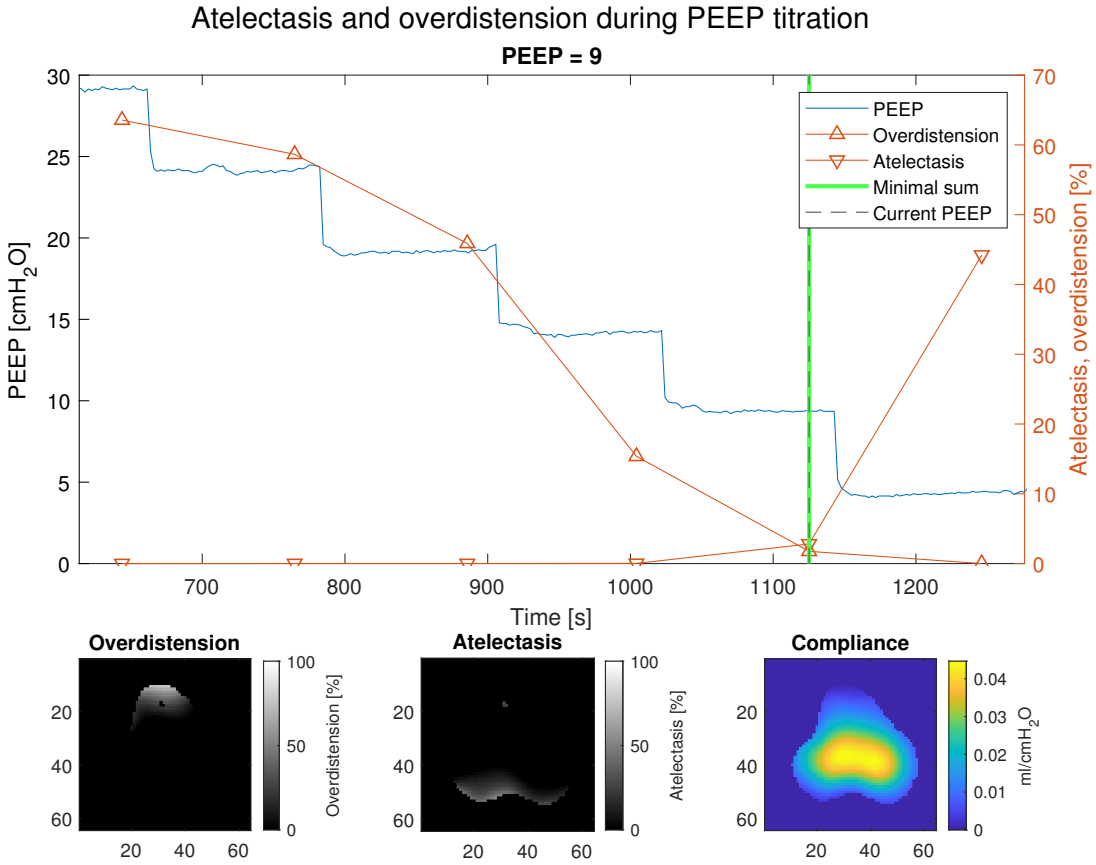

Figure 3.12: Single slice from the animation available in thesis documentation. Above, PEEP and compliance values from the ventilation data are plotted. Below, images show overdistension, atelectasis (percentage-based), and regional compliance at a given PEEP level, respectively.

Overdistension is defined in the same way as atelectasis (see Equation 3.8), with the difference that the value is set to zero for pixels that already have passed the highest compliance.

The collective atelectasis or overdistension values for the whole image are calculated based on the individual pixel percentual values, weighted by the best compliance achievable for a given pixel. The product of pixel percentages and weights are consequentially summed and divided by the sum of all pixels' best compliance values. Thus, the cumulated value for each PEEP level expresses the percentual amount of atelectasis or overdistension out of a hypothetical image, where every pixel has the best compliance value achievable over the PEEP titration.

Equation 3.9 shows the definition of cumulated collapse, $\text{Collapse}_{\text{frame}}$.

$$\text{Collapse}_{\text{frame}}\,(\%) = \frac{\sum_p \left(\text{Collapse}_p \times \text{C}_{\text{best},p}\right)}{\sum_p \text{C}_{\text{best},p}} \tag{3.9}$$

Pseudocode for the calculation of atelectasis and overdistension following the definition by Costa et al. [37] is provided in Algorithm 1.

3.4.3 Feature normalization

To provide an overview of correlation or similarity among the features, they were normalized and plotted. Simultaneously, the sum of all features per PEEP level was plotted. Normalization was performed in a way that a higher normalized value agreed with a better outcome. Compliance, CoG and CoV were scaled to [0,1] using their minimal and maximal values over the titration. In the case of atelectasis and overdistension, their sum was scaled to [0,1] as well, with the highest value corresponding to 1, but zero kept at 0 % atelectasis and overdistension.

That provided a useful insight. However, the selection of normalization ranges and ideal values was somewhat arbitrary, and their adjustment impractical. Therefore, a small utility was designed using Matlab App designer. Even though the implementation was not completed, the utility provided a simple visualization of the impact of scaling and weighting on features and the resulting "best performing" PEEP level. Nevertheless, the normalization served as an outline for the next step, fuzzification.

Algorithm 1 Atelectasis and overdistension

Input:
matrix C of local compliance.

Output:
matrix A of local atelectasis,
matrix O of local overdistension,
array A_{frame} of cumulated atelectasis,
array O_{frame} of cumulated overdistension.
▷ Size of C, A, and O is $[f, p]$, where f is the number of frames (PEEP steps), and p is the number of pixels

procedure AtelectasisOverdistension(C)
  for $i \leftarrow 1$ to p **do**
    $C_{\text{best}}(i) \leftarrow \max(C(:, i))$
    $C_{\text{best,idx}}(i) \leftarrow$ index of the best compliance value frame f
  end for
  for $i \leftarrow 1$ to f **do**
    for $j \leftarrow 1$ to p **do**
      if $i > C_{\text{best,idx}}(j)$ **then**
        $A(i, j) \leftarrow (1 - [C(i, j)/C_{\text{best}}(j)]) \times 100$
      else
        $A(i, j) \leftarrow 0$ ▷ Has not reached the best compliance yet.
      end if
      if $i < C_{\text{best,idx}}(j)$ **then**
        $O(i, j) \leftarrow (1 - [C(i, j)/C_{\text{best}}(j)]) \times 100$
      else
        $O(i, j) \leftarrow 0$ ▷ Has already reached the best compliance.
      end if
    end for
  end for
  for $i \leftarrow 1$ to f **do**
    $A_{frame}(i) \leftarrow \frac{\sum_{j=1}^{p} A(i,j) \cdot C_{\text{best}}(j)}{\sum C_{\text{best}}}$
    $O_{frame}(i) \leftarrow \frac{\sum_{j=1}^{p} O(i,j) \cdot C_{\text{best}}(j)}{\sum C_{\text{best}}}$
  end for
end procedure

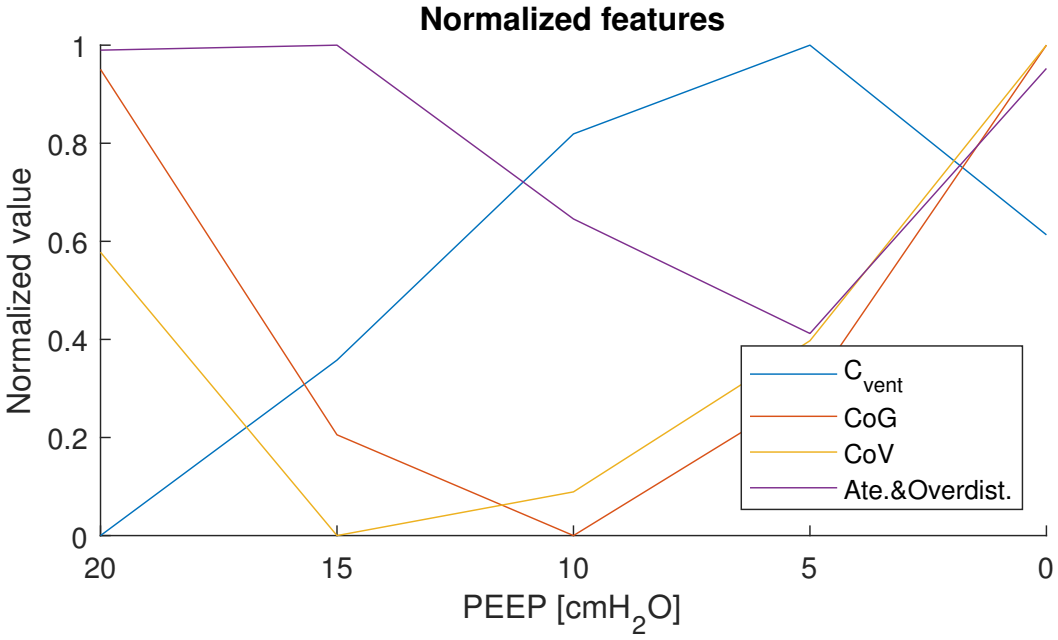

Figure 3.13: Features normalized to the range between minimum and maximum value from the titration. In this example, both compliance and atelectasis and overdistension exhibit their best value (highest and lowest, respectively) at PEEP of 5 cmH_2O, while CoG and CoV at higher PEEP values. A slight difference in CoG and CoV can be observed.

Figure 3.14: GUI of feature normalization utility allows user to select normalization limits and weights for individual features. Note that the values are arbitrary in this example.

3.5 Fuzzy inference system

In order to evaluate the ventilation performance at every PEEP level, a fuzzy inference system (FIS) was implemented. At the input side of the system, there were the values of EIT-derived features, atelectasis, overdistension, CoG, and CoV, while the system produced a single value in a range from 0 to 1, representing the performance. Figure 3.15 shows an overview of the system.

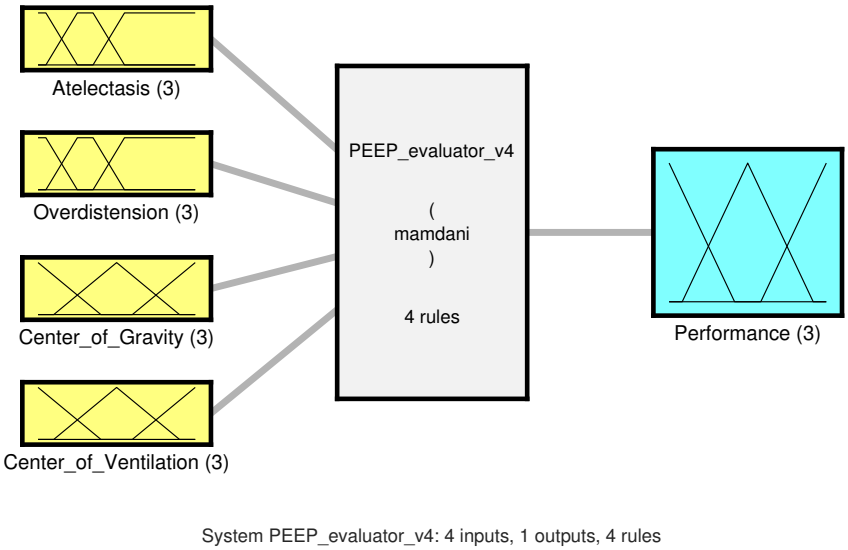

Figure 3.15: Structural overview of the fuzzy inference system used for PEEP evaluation.

Atelectasis and overdistension were not scaled - the percentual values between 0 and 100% were used as an input. Three trapezoidal membership functions (MF) were designed for atelectasis fuzzification (Figure 3.16). The same set of MFs was used for overdistension.

Both CoG and CoV values were scaled to range between 0 and 1 with respect to their minimal and maximal values. Again, the same set of MFs was used for both features. Three triangular MFs were designed for CoG and CoV (Figure 3.17).

The output uses MFs with the same parameters as CoG and CoV, only with different names (Figure 3.18).

In total, only four rules were implemented in the system. The rules are summarized in Table 3.3. Rules were assigned uniform weights.

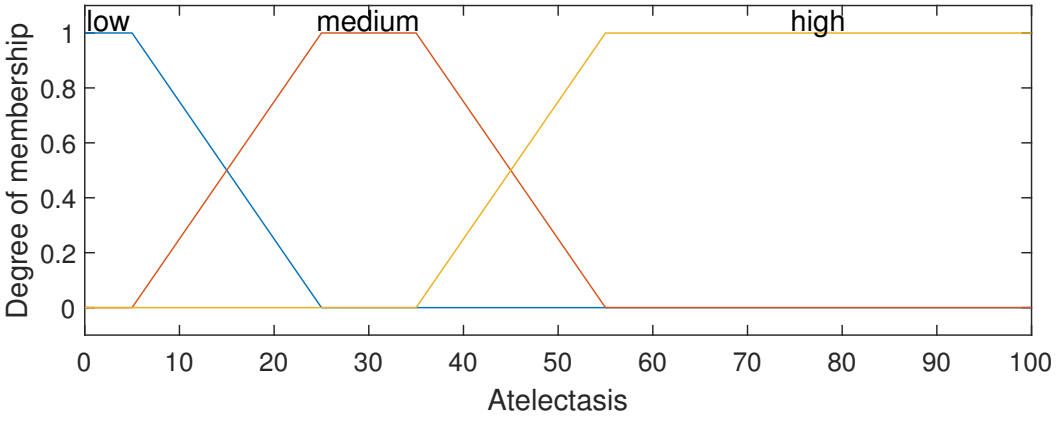

Figure 3.16: Fuzzy membership functions used for fuzzification of atelectasis and overdistension.

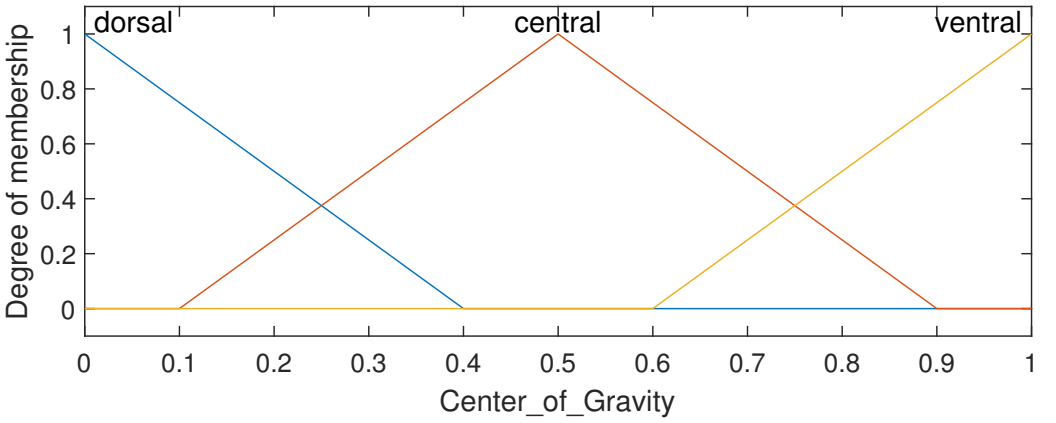

Figure 3.17: Fuzzy membership functions used for fuzzification of center of gravity and ventilation

Table 3.3: Overview of FIS rules.

Rule	Method[a]	Atelect.	Overdist.	CoG	CoV	Performance
1	AND	low	low	dorsal	dorsal	excellent
2	OR	high	high	ventral	ventral	poor
3	OR	high	high	central	central	NOT excellent
4	OR	low	low	dorsal	dorsal	excellent

[a] Logical connection between individual features to form the rule.

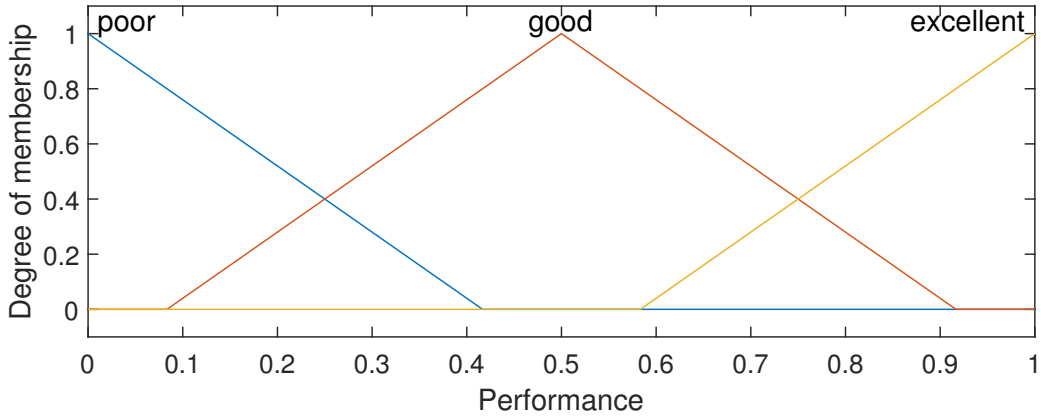

Figure 3.18: Fuzzy membership functions used for defuzzification of the system's output.

4 Results and discussion

In this section, results for intermediate calculations and features are presented and discussed, followed by general comments and results of the fuzzy inference system towards the end of the chapter. As described in the Dataset description, only five measurements passed the initial preprocessing (see highlighted in Table A.2 in Appendix). The small size of the dataset has to be considered for the results presented here.

All results are presented for subject E, with eventual differences or outstanding results shown for respective subjects.

4.1 Intermediate results

The PEEP titrations were recorded in 5 cmH_2O steps. Although the differences between steps agree, the absolute values of PEEP follow the form $5n - 1$, where $n \in \mathbb{N}$ for some measurements. No corrections were implemented, as this does not affect the calculations.

The lung mask proved to be capable of eliminating artifacts in further calculations, especially in the case of atelectasis and overdistension. An example of the resulting mask is depicted in Figure 4.1. Consequently, the individual masks were significantly smaller for better performing PEEP levels due to the increased quarter amplitude set threshold.

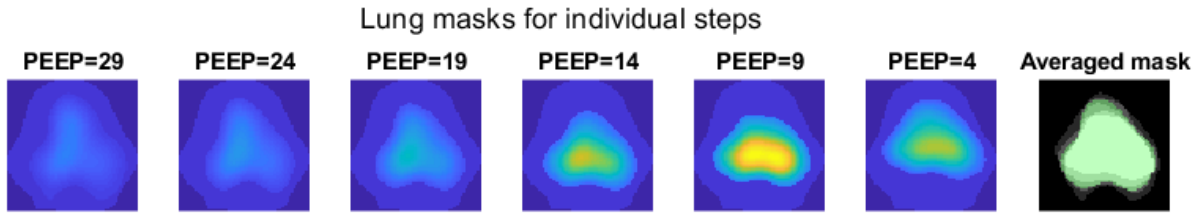

Figure 4.1: Individual lung mask at all PEEP levels for subject E. Right: summed individual masks, the light green area represents the resulting averaged mask.

While it is convenient to use the averaged lung mask for the calculations, it does not necessarily represent the lungs' correct shape. Furthermore, the threshold value for pixel inclusion, in turn, determines at how many PEEP levels the pixel has to perform well compared to the whole image in order to be part of the mask. If a titration with many PEEP steps was to be used, and dorsal regions were only properly ventilated during a short range of PEEP values, the corresponding pixels would not appear in the mask unless a low enough threshold was used.

The ventilator data only provide one feature for the titration assessment, which is respiratory compliance. Figure 4.2 shows the compliance values as calculated for every breathing cycle of a PEEP titration. Compliance follows a typical trend, with an initial decrease as PEEP rises and the upside-down "U" shape during the decreasing section of the titration. The peaks are introduced by pressure and flow fluctuations following the PEEP change.

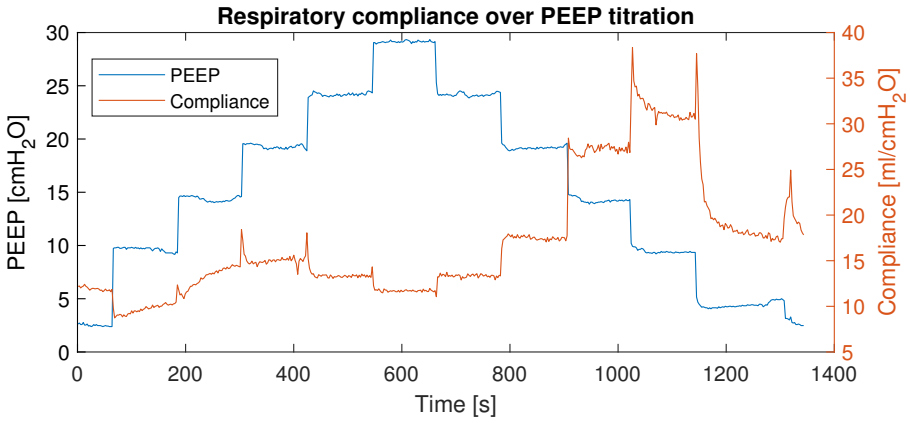

Figure 4.2: Respiratory compliance calculated from the ventilation data displayed over the PEEP values. Note that the peaks are caused by pressure and flow fluctuations following the PEEP change.

Although the global respiratory compliance provides a simple lung performance evaluation, it is not able to cover the underlying local changes as described in Motivation and confirmed later in this section.

4.2 Compliance bands

Compliance bands (Figure 4.3) provided a very intuitive overview of the regional lung performance, as they highlighted the regional compliance in relation to the ventral-to-dorsal axis.

Furthermore, when the differential TV images were used, the inter step changes in compliance were even better visible (Figure 4.4). As the PEEP decreases, compliance loss starts to occur in the dorsal regions first. On a global scale (the compliance value extracted from the ventilator data) the compliance would still increase, due to further increase in the central regions of the lungs, while the dependent regions start to collapse.

This inspired an idea of a feature (or rather a rule) to be used to choose the ideal PEEP value. Given no (or limited) compliance loss is allowed, the last PEEP level that precedes the compliance loss in the dependent region would be assigned higher importance. However, this rule was not used in the final fuzzy system (details below).

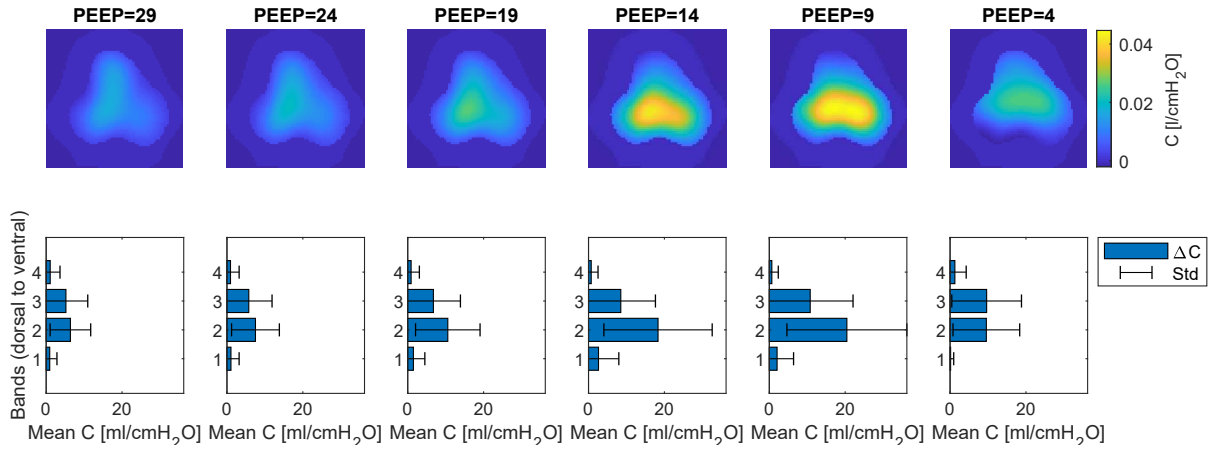

Figure 4.3: Tidal variation images with corresponding mean compliance values of four bands, vertically dividing the image. Subject E.

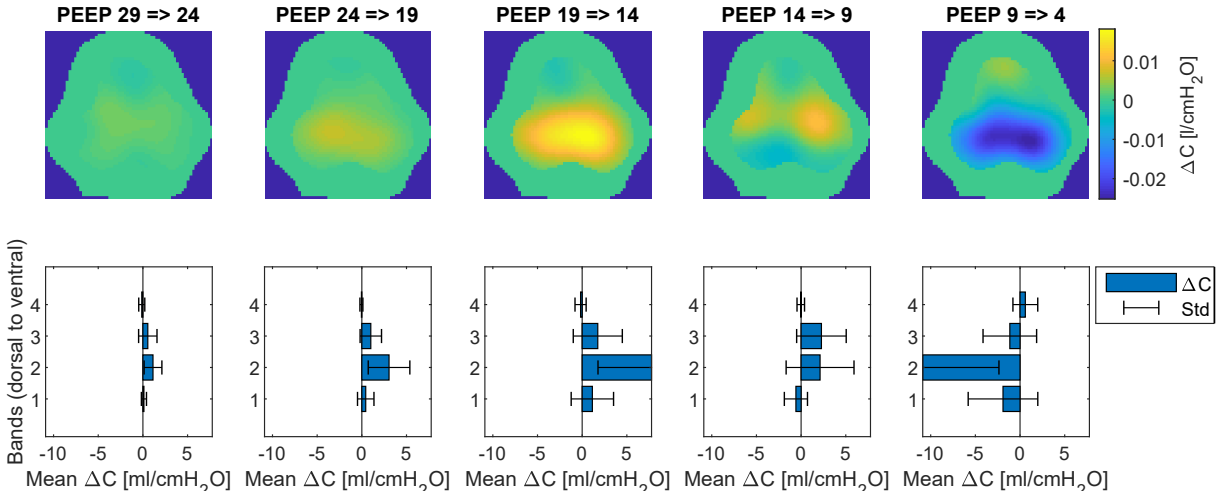

Figure 4.4: Differential tidal variation images for consequent PEEP levels. Bars represent the average compliance gain/loss for the respective band. Subject E. At PEEP step from 14 to 9 cmH_2O, compliance loss can be seen in the dorsal region, which is also apparent from the bar plot below.

The bands' position and width were fixed on the whole pig thorax, regardless of the lung mask. This led to a minimal number of pixels, especially in the dorsal-most band, for some measurements. The argument supporting fixed bands is that if there is no ventilation in the dorsal band, the ventilation performance is weak in the region regardless of the PEEP value. Nonetheless, it is vital to consider the algorithm for lung mask calculation and the corresponding threshold for pixel inclusion (mentioned above).

However, all other features are calculated with respect to the lung mask and therefore individualized for each subject. If the bands were uniformly distributed over the lung mask's height, the results would be individualized in this case as well.

4.3 Center of gravity and ventilation

Center of gravity and center of ventilation both provide a single value as a result. Although each of the metrics provides slightly different results, depending on the shape of the histogram of row sums (Figure 4.5, note that the changes in CoG and CoV are in order of units of percents), the values are well correlated (discussed below). Figure 4.6 shows course of both CoG and CoV as compared to compliance.

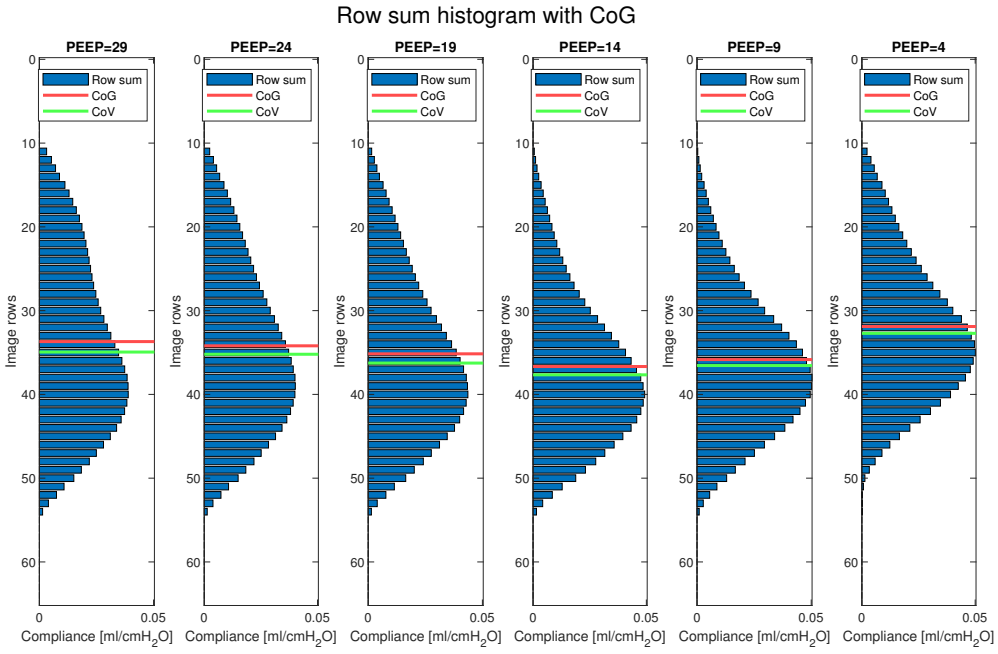

Figure 4.5: Row sums of tidal variation images with centers of gravity and ventilation annotated at all PEEP levels for subject E.

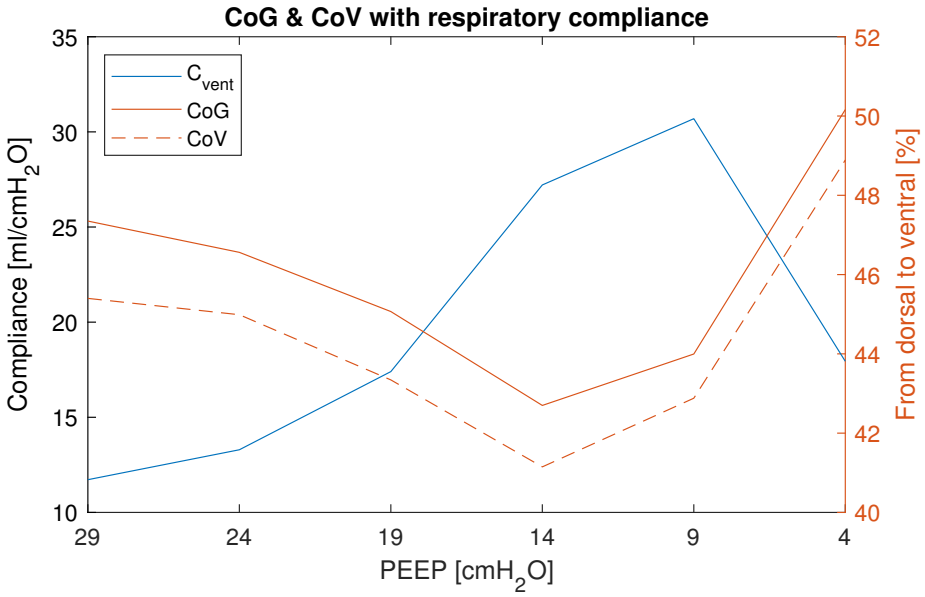

Figure 4.6: Comparison of global compliance and center of gravity and ventilation values. Although there is an increase in global compliance between steps with PEEP of 14 and 9 cmH_2O, the increase in CoG and CoV values suggests that the increase in compliance does not occur in dorsal regions.

Single values produced by CoG and CoV are easy to process, however harder to interpret since it suffers from a problem similar to the global compliance - simultaneous increase or decrease on opposite sides of lungs leads to no change in the resulting value (in case of compliance, the opposite effects in different parts of lungs cancel each other out).

Furthermore, rows with a small compliance sum compared to the whole lung area have only a limited effect on the resulting value even when located at the axis extremes (dorsal- or ventral-most). Nevertheless, the compliance changes in dorsal regions surpassed the changes in ventral regions in most examined subjects. Thus the CoG and CoV values were shifted towards the dorsal end.

From the examination of aligned values of all features calculated, CoG always (with the exception of subject C, where CoG slightly increases between PEEP 19 and 9) exhibits local minima one PEEP level before the maxima in global compliance. The number of steps in each titration is too small to perform reliable lag analysis (e.g., cross-correlation).

Compared to differential TV images or atelectasis and overdistension, CoG and CoV are harder to interpret. As described above, complex changes might hide behind small variations of the value. Blankman et al. [38] chose the lowest value (the dorsal-most) as the best performing. The reasoning is that the shift towards the back reflects the recruitment of the dependent dorsal regions.

CoG and CoV were calculated without regard to the lung mask. As a result, a truly balanced TV image would not necessarily yield a value of 50%. Nevertheless, the shift that is introduced by the lung mask is constant for all PEEP levels of a given titration since the mask is constant as well. Therefore only the changes in the CoG and CoV values are essential for the evaluation.

4.4 Atelectasis and overdistension

Atelectasis and overdistension were initially calculated on a pixel basis. At each PEEP level, every pixel was classified as either atelectatic, regular, or overdistended. The number of pixels of every class was then counted and divided by the total number of pixels in lung ROI to express the value in percent.

The later implemented method depended not only on the number of classified pixels but on their best compliance throughout the titration. Every pixel was assessed based on the relation of its current value compared to the best one. If it was classified as non-ideally ventilated, the value was expressed in percent of the best value directly. The cumulated overdistension or compliance for a PEEP level was then calculated as a weighted sum of individual pixel percentages, where the weighting factor was the best compliance value of each pixel. Therefore, areas that contributed more to global compliance got more importance when classified atelectatic or overdistended. Consequently, the second method produced higher percentual values for the steps with a higher portion of non-ideally ventilated pixels (caused by the big influence of high-compliance pixels) and lower percentual values for PEEP levels with only the peripheral pixels non-ideally ventilated.

Results of both methods are compared below (see Feature correlation and Fuzzy inference system). Figure 4.7 shows the downward PEEP titration in terms of percentage-based atelectasis and overdistension.

In all examined subjects, the minimal value of atelectasis and overdistension sum corresponded with the maximum in global compliance for both the pixel-based and percentage-based method. Furthermore, the correlation between respiratory compliance and both pixel-based and percentage-based atelectasis and overdistention sum was significant (the percentage-based with p-value $<= 0.01$ for all subjects). This can be explained by the fact, that both methods rely on the compliance value course. Both algorithms expect the compliance of every pixel to follow the "hat" curve during the downward titration, while overdistension is classified before reaching maxima and similarly atelectasis after reaching the maxima of the pixel compliances. Figure 4.8 shows the course of local compliance for approximately 100 randomly selected pixels of lung area ROI. It can be seen, that the curves exhibit their maxima in a small range of PEEP levels.

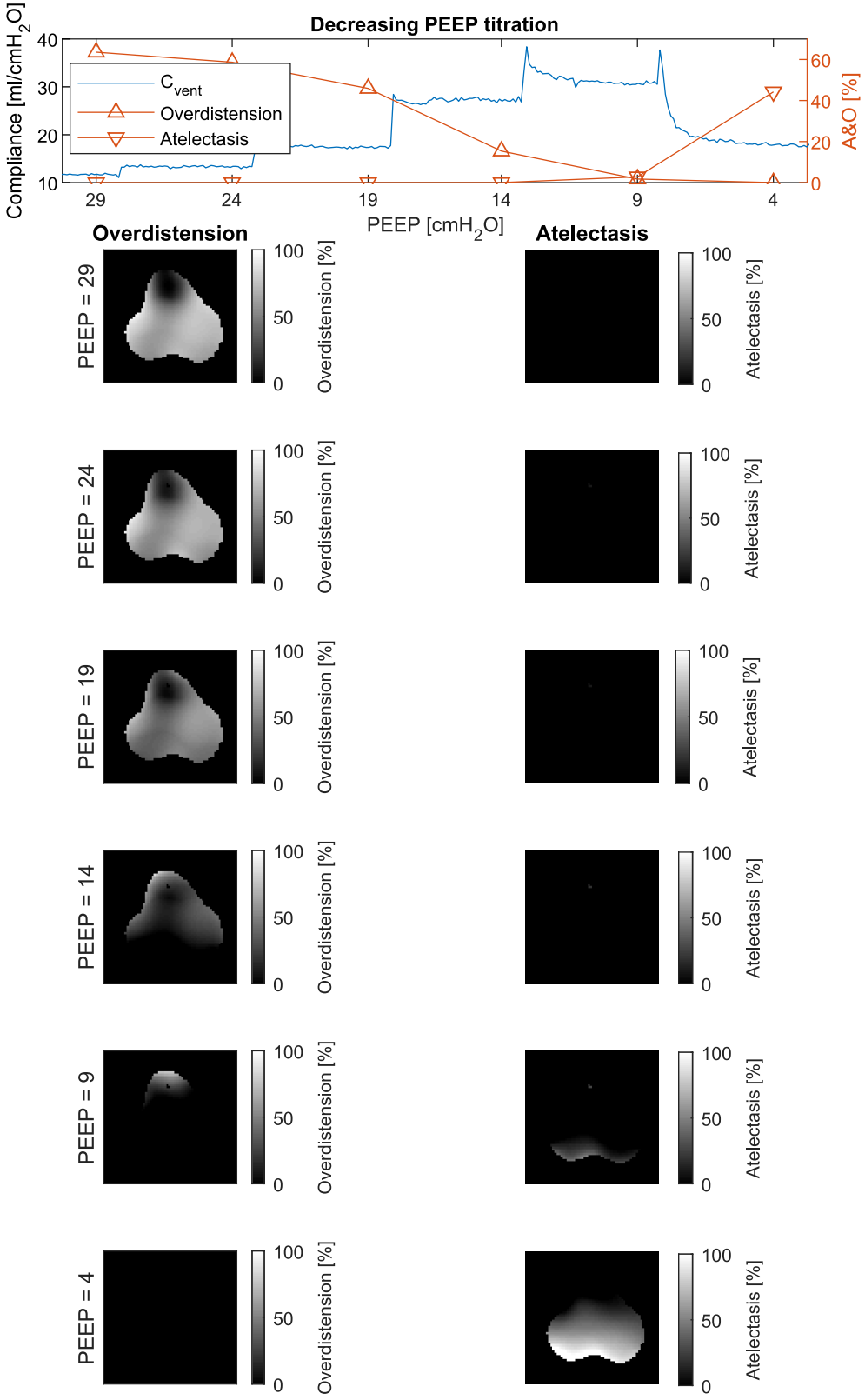

Figure 4.7: Atelectasis and overdistension values along with the global compliance for downward PEEP titration in subject E. The images show atelectasis and overdistension expressed in percent compared to the best achievable compliance for each pixel. Note that there is no PEEP level with perfectly ventilated regions.

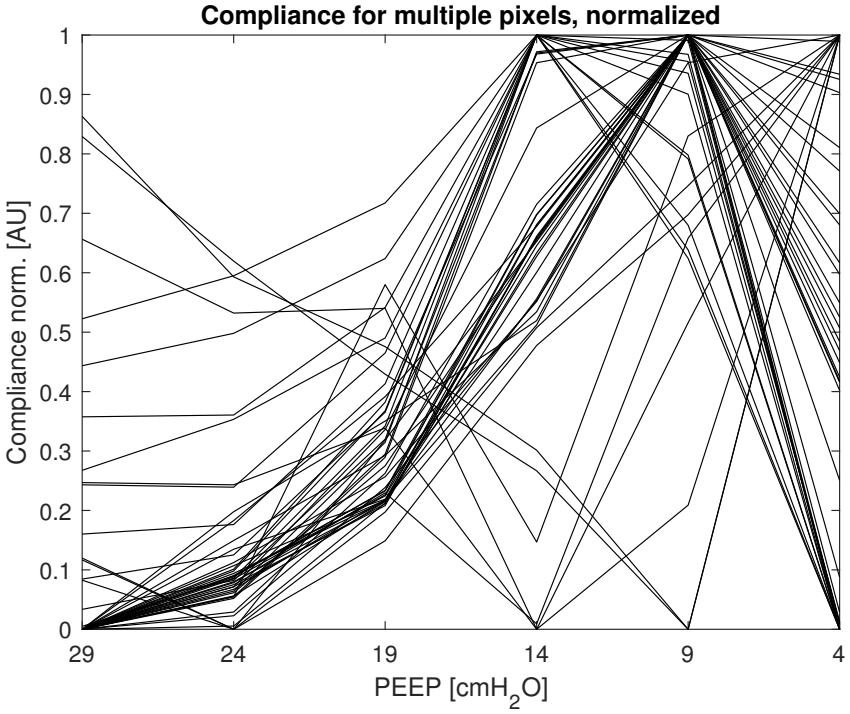

Figure 4.8: Normalized compliance values for ca. hundred randomly selected pixels. The majority of pixels exhibit maxima at one of two consequent PEEP levels.

The definition of atelectasis and overdistension as implemented in this thesis brings one more dependency, which is the PEEP range over which the atelectasis and overdistension values are calculated. As illustrated in Figure 4.9 from Zhao et al. [36], the results will differ for different PEEP ranges. This happens because the classification is driven by the global maxima of compliance for each pixel.

4.5 Feature correlation

As already mentioned, features exhibit high correlation. Figure 4.10 shows the correlation matrix and corresponding p-values for combination of all feature vectors, where correlation coefficient is Pearson's linear correlation coefficient r, defined as

$$r(x,y) = \frac{\sum_{i=1}^{n}(x_i - \bar{x})(y_i - \bar{y})}{\sqrt{\sum_{i=1}^{n}(x_i - \bar{x})^2}\sqrt{\sum_{i=1}^{n}(y_i - \bar{y})^2}}, \tag{4.1}$$

where n is the length of vectors x and y, and $\bar{x}$ denotes the mean value of vector x. P-value is the significance level of a nonzero correlation.

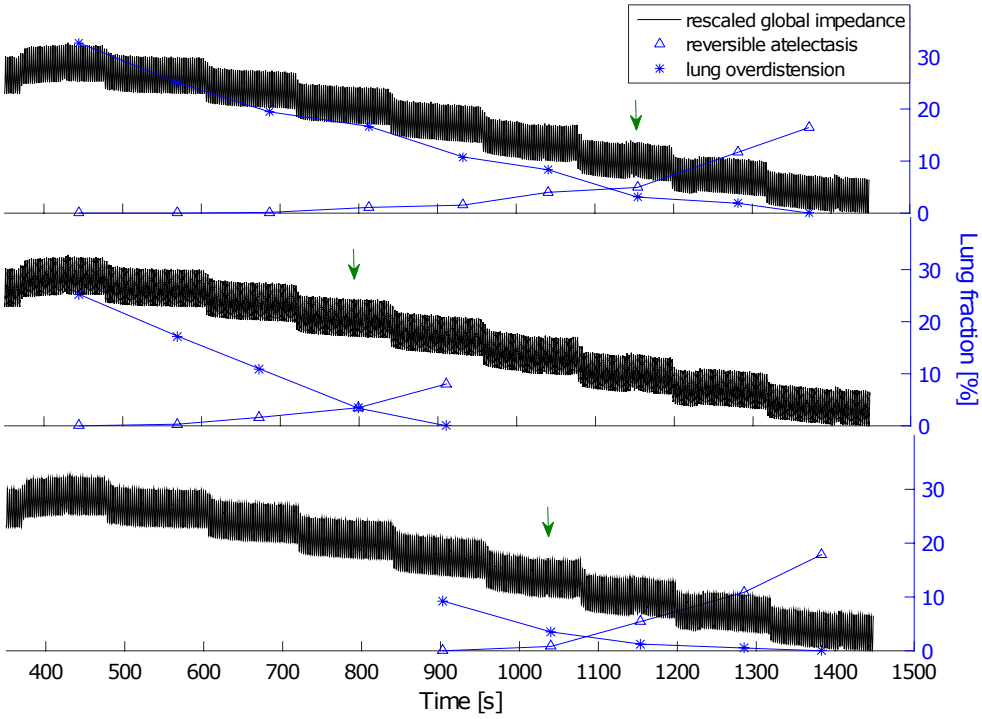

Figure 4.9: Influence of PEEP step range selection on resulting atelectasis and overdistension values, from [36].

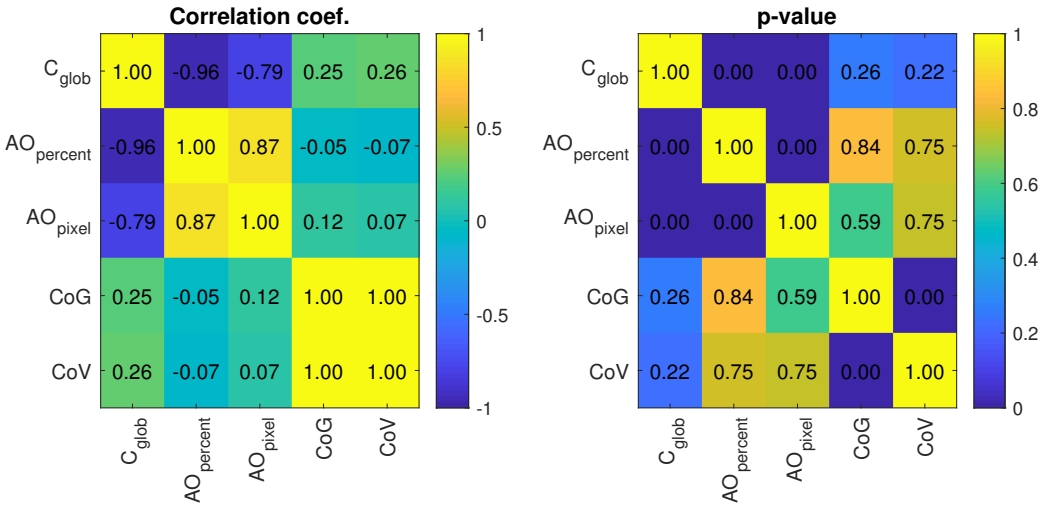

Figure 4.10: Correlation matrix and corresponding p-values for combination of all feature vectors.

Another feature that could have been introduced into the system was the global inhomogeneity (GI) index. As the name suggests, the GI index aims to quantify ventilation inhomogeneity. The definition measures the inhomogeneity in terms of a sum of absolute differences between individual pixel values and the median value for a given TV image. The lowest value corresponds with the highest homogeneity and is therefore considered optimal.

However, Zhao et al. showed a high correlation of GI index with global compliance [39], and since it does not offer any added value as in the case of atelectasis and overdistension, it was not added to the feature set.

4.6 Interpretation

The author of this thesis has no medical education. The interpretation of results and conclusions derived in this thesis would have to be verified by medical experts and further research. The best ventilation performance, as evaluated in this thesis, is focused on the successful recruitment of dependent lung regions.

Atelectasis and overdistension values provide a very intuitive assessment of the titration. However, as shown in the previous section, there is a high correlation among the features. Specifically, in the case of the sum of percentage-based atelectasis and overdistension, there was no added value as compared to ventilator-derived respiratory compliance. For an automated evaluation, it is not enough to only consider the percentage of non-ideally ventilated lung regions (the sum of percentual overdistension and atelectasis), as it does not provide added value (due to the correlation with global compliance shown above).

In the analyzed measurements, CoG and CoV systematically exhibit minima (the dorsalmost position) one step before the maxima in global compliance (Figure 4.11). This might be explained by the successful recruitment of the dependent lung areas, which shifts the CoG and CoV back. While the global compliance further increases at the next PEEP level, the center of gravity and ventilation increases as well, suggesting that the increase in compliance occurs in a "wrong" lung region or that the dependent regions start to collapse. Atelectasis data further support this idea. Even though the minimal sum of atelectasis and overdistension corresponds with the global compliance maxima, all of the processed measurements exhibited an increase in atelectasis preceding the highest compliance step. This increase corresponds to the loss of recruitment in the dorsal regions. Figure 4.12 illustrates the idea of results for one of the processed subjects.

Figure 4.13 shows one more example, where downward PEEP titration is followed by one PEEP increase. Among other things, it illustrates the pressure-volume relation hysteresis, as decrease compliance at zero PEEP is much bigger than the increase achieved after the increase in PEEP. In terms of the P-V curve, this would mean following the upper path

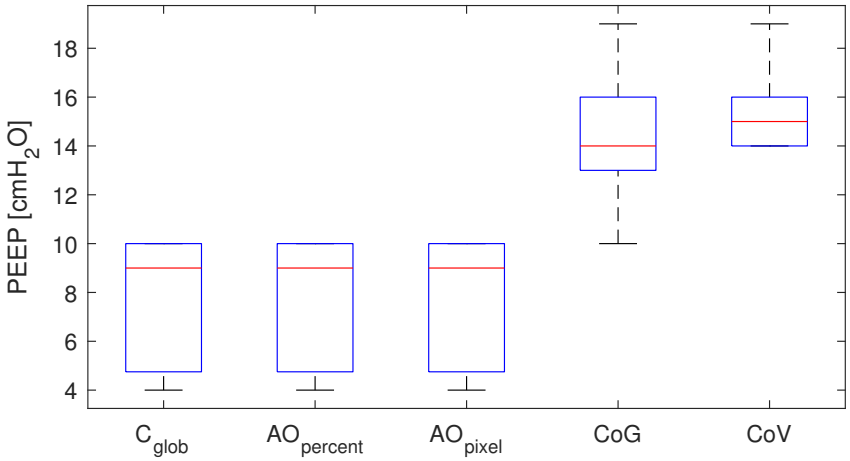

Figure 4.11: Boxplot comparing predicted PEEP values based on various features for all measurements analyzed. C_{glob} means maximal value of global compliance, $AO_{percent}$ and AO_{pixel} mean percent-based and pixel-based atelectasis and overdistension respectively, CoG and CoV stands for center of gravity and ventilation respectively.

down to the origin and then increasing the pressure, however, following the lower path without a comparable gain in volume.

The presented method has a notable downside - the evaluation only works off-line. All features and, therefore, the evaluation depend on the knowledge of the highest values of several parameters over the complete titration. In turn, the evaluation can only be calculated once the titration is completed down to zero PEEP.

4.7 Fuzzy inference system

Results obtained from the FIS further support the idea that the ideal PEEP value is higher than the one suggested by the highest global compliance. Percent-based atelectasis and overdistension, CoG and CoV were used for the evaluation. For every PEEP level, the performance was evaluated, using current feature values.

The system, however, only applies the defined rules. These rules were adjusted in several trial and error attempts until the results were consistent among all subjects and exhibited a single significant peak for every subject. See the Outlook section for more comments on the usability.

Figure 4.14 shows courses of all features during the downward titration in subject E. This visually illustrates the correlation of global compliance with atelectasis and overdistension sums and the alignment of valley in CoG and CoV values with peak in FIS output. Peak

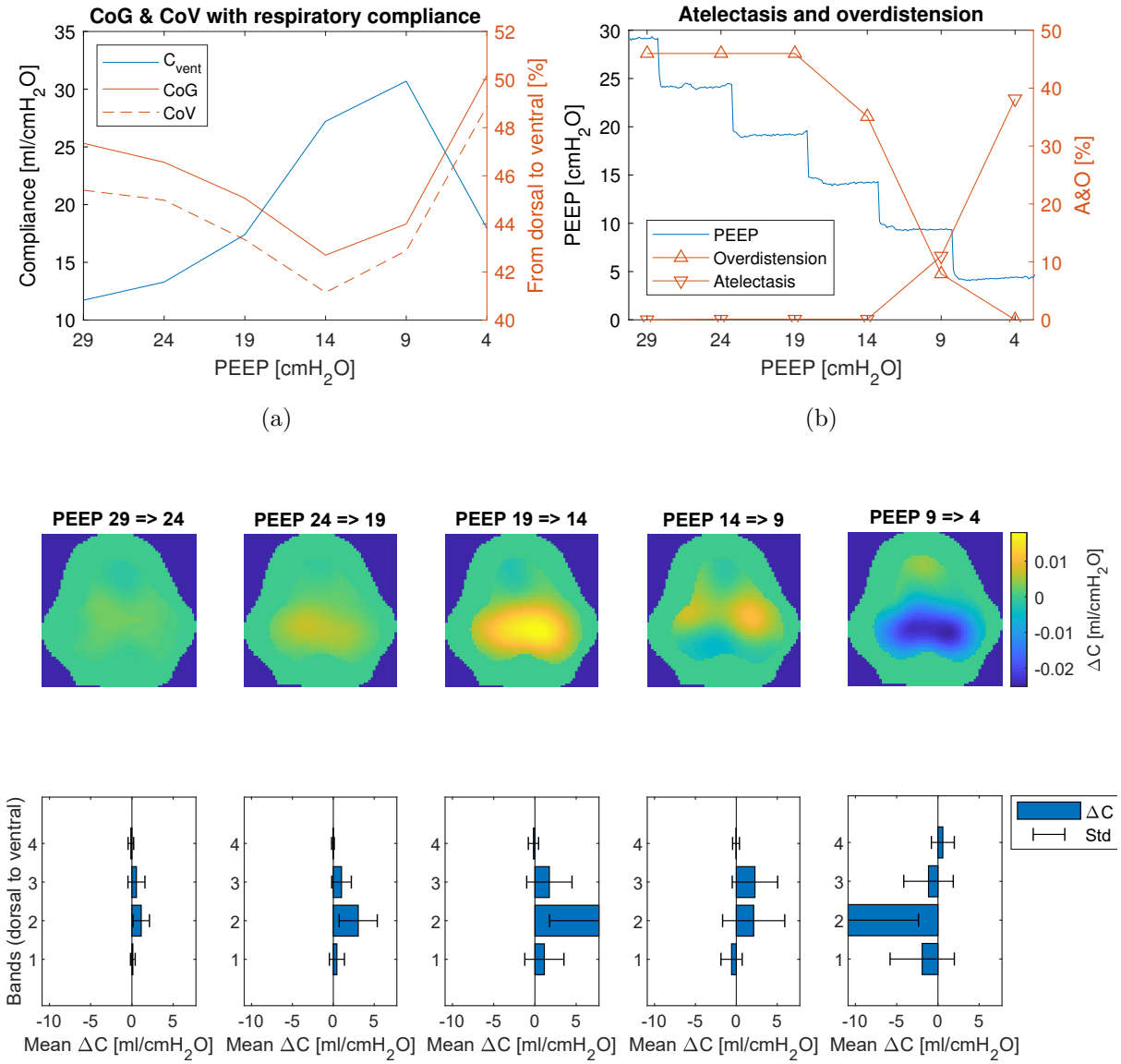

Figure 4.12: Results for subject E, (a) CoV and CoG, (b) atelectasis and overdistension, (c) differential tidal variation, and mean compliance bands. The minimal value of CoG at PEEP of 14 cmH_2O corresponds with the highest compliance in the dorsal region and almost no atelectasis. While global compliance increases as PEEP changes from 14 to 9 cmH_2O, the dorsal regions exhibit collapse, supported by increased atelectasis and rising CoG.

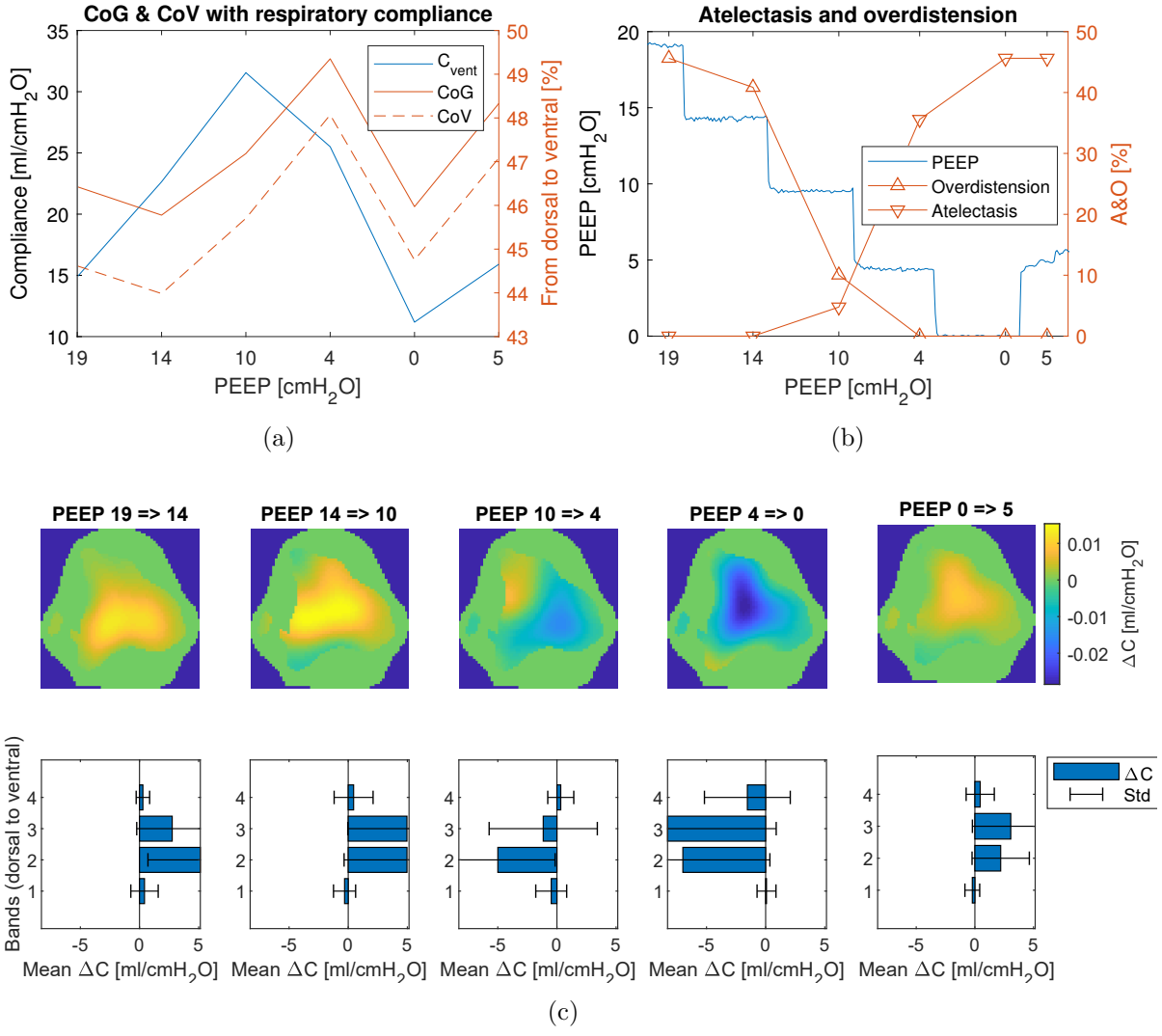

Figure 4.13: Results for subject C, (a) CoV and CoG, (b) atelectasis and overdistension, (c) differential tidal variation, and mean compliance bands. After the titration reached zero, PEEP was increased to 5 cmH_2O again. Similarly to subject E, compliance reaches its maximum at PEEP of 10 cmH_2O, while best dorsal recruitment (local minimum of CoG) occurs one step earlier. The rise in CoG and CoV between steps 14 and 4 shows that the ventilation shifts up, however as the PEEP gets to zero, it shifts back, likely caused by uniform lung collapse. The subsequent increase in PEEP is accompanied by an increase in both compliance and center of gravity, suggesting that the dependent areas do not reopen easily.

in FIS performance evaluation corresponded with the step preceding the highest global compliance in all analyzed subjects. Evaluations of all subjects are summarized in Table 4.1, figures with aligned features for all subjects are attached in Appendix A.1, A.2, A.3, and A.4.

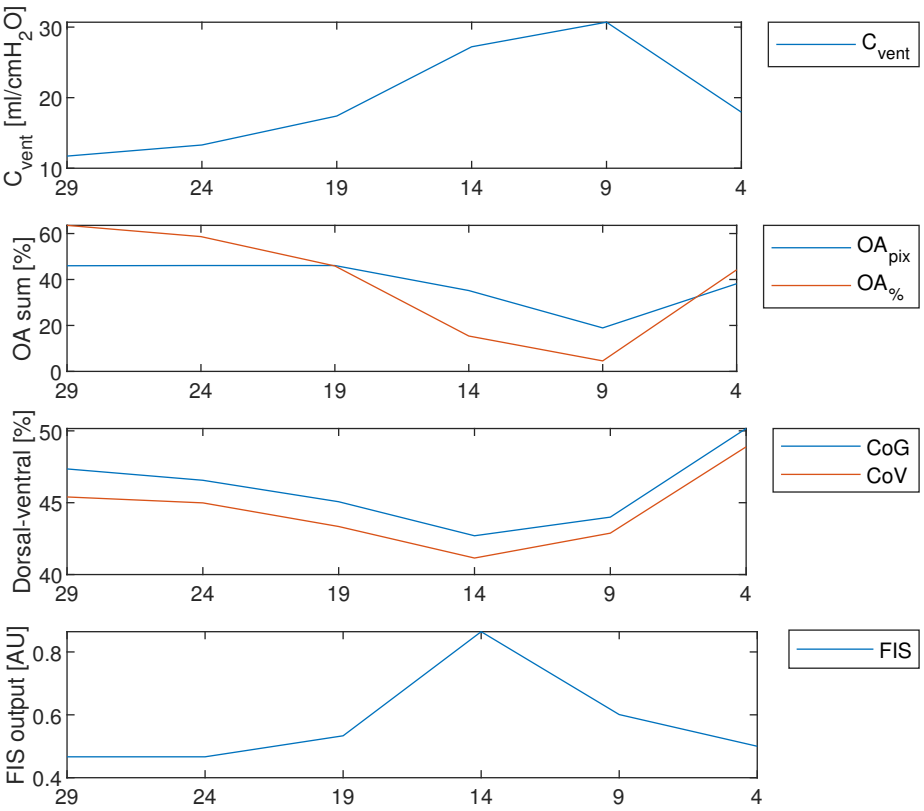

Figure 4.14: Alignment of features and evaluation of FIS. Global compliance corresponds with atelectasis, and overdistension sums, the position of the lowest point in CoG and CoV values agrees with the peak in FIS output.

Table 4.1: Results of FIS evaluation for all subjects. Values corresponding to the highest global compliance are marked with an asterisk.

PEEP	FIS evaluation				
	A	B	C	D	E
30	-	-	-	-	0.466
25	-	-	-	-	0.466
20	0.466	0.513	0.468	0.466	0.533
15	0.622	0.864	0.864	0.658	0.864
10	0.864	0.662*	0.491*	0.706	0.601*
5	0.500*	0.481	0.500	0.500*	0.500
0	0.500	0.483	0.466	0.544	-
5	-	-	0.487	-	-

5 Conclusions and outlook

This thesis presented an EIT-based PEEP titration evaluation built on several local features. The solution starts with EIT data processing using the EIDORS library and continues with feature generation. The evaluation is finally generated in a fuzzy system, which combines all the features.

As one of the results presented in this thesis, a decrease of compliance in dorsal regions accompanied by the onset of atelectasis was observed, while the global compliance increased for one more downward step in PEEP. This supports the assumption that the local information could provide a better evaluation of ventilation performance.

It was also shown that the sum of atelectasis and overdistension is highly correlated with global compliance, as its definition depends on it. Thus, there is no added value in the sum of the two, and atelectasis and overdistension should be treated as two individual features.

However, it also illustrated the loss of information in the global parameter. In the case of atelectasis and overdistension, the opposite effects are particularly apparent. When PEEP decreases, the previously overdistended regions contribute to compliance increase, while other regions collapse and decrease global compliance. The global compliance value can, therefore, only identify the best trade-off between the two processes.

Statistical analysis was performed to a limited extent due to the minimal number of processed subjects. Analysis of a greater number of measurements would be necessary to validate the presented processing chain and enable a more reliable interpretation of the results.

Further investigation and expert knowledge are needed, should the system be further developed or used.

The titration with PEEP steps of 5 cmH_2O is likely too coarse to cover the actual ideal PEEP value. Step-to-step differences are very steep close to the best performing value, but as data suggest (see Figures 3.10 and 4.8, note the two similar well-performing PEEP levels), the ideal value might lie between the recorded steps. Recording with steps of 2 cmH_2O could identify a closer-to-ideal value.

There are many possibilities to further extend the system. The goal of this thesis was to provide an evaluation from the perspective of lung mechanics. However, ideal lung mechanics do not necessarily guarantee the best outcomes for the patient. Physiological measurements and parameters like blood oxygen saturation and carbon dioxide elimination could be incorporated to evaluate the titration in terms of the gas exchange. Adding

more features not so closely correlated to global compliance could improve the system's robustness.

With further data to analyze, complex feature linkages could be potentially exploited. This could enable the system not only to perform an on-line evaluation but possibly also to predict the ideal PEEP value and stop the titration without the need to finish it. Reducing the time spent at unnecessary high PEEP levels would lower the harm and risks for the patient.

There are several parameters and thresholds throughout the system which were chosen empirically. Better values could be found by running the analysis multiple times over the parametric space and analyzing the effects of individual parameter value combinations.

Even though the number of features processed in this thesis is not excessive, the processing part and the calculated features could serve as a basis for further, closely focused theses.

A Appendix

The code, figures, and results are provided on a physical medium attached to the thesis printout. The original dataset can be provided by MedIT[1]. Table A.1 describes the structure of the files attached to the thesis.

Table A.1: The folder structure of the attached files.

Folder	Contents
code	All scripts and functions used to process, visualize and evaluate the data.
data	The dataset tracking table (basis for Table A.2).
figures	Generated figures and results. The folder structure is as follows: *<dataset name>/<measurement name>/<filename>/<results>*
images	Additional images and the original figures that are used in the thesis.

Furthermore, a summary of data preprocessing is provided in Table A.2. Finally, results for all processed files are provided. Please refer to the respective chapter for details.

[1] Chair for Medical Information Technology, Helmholtz Institute, RWTH Aachen University, Pauwelsstr. 20, D-52074 Aachen, www.medit.hia.rwth-aachen.de

Table A.2: Tracking table between the original dataset structure and the structure used in processing.

Date	EIT file	Ventilab file	New name	ID	EIT preview
2005-04-01	Schwein2010405_Rampe1_01_001.get	Rampe1.fpv	Rampe1	A	OK
2005-04-01	Schwein2010405_Rampe2_01_001.get	Rampe2.fpv	Rampe2	B	OK
2005-07-02	-	-	-	-	Unable to load
2005-07-03	-	-	-	-	Unable to load
2005-07-04	-	-	-	-	Unable to load
2005-07-05	-	-	-	-	Unable to load
2005-07-06	-	-	-	-	Unable to load
2005-08-30	ARDS_300805_rampe 1_01_.eit	Dur1.fpv	rampe1	C	OK
2005-08-31	ARDS_310805_ards_rampe 1_01_.eit	Dur1.fpv	rampe1	D	OK
2005-08-31	ARDS_310805_Ards_rampe 2 (post Lavage)_01_.eit	dur2.fpv	rampe2	E	OK
2005-09-01	ARDS_010905_rampe 1_01_.eit	dur1.fpv	rampe1	-	Artifacts
2005-09-01	ARDS_010905_rampe 2a_01_.eit	Dur2.fpv	rampe2	-	Artifacts
2005-09-02	ARDS_010905_rampe 1 healthy_01_.eit	Dur1.fpv	rampe1_healthy	-	Artifacts
2005-09-02	ARDS_010905_rampe 2_02_.eit	Dur2.fpv	rampe2	-	Artifacts
2005-09-02	ARDS_020905_rampe 2a_01_.eit	Dur3.fpv	rampe3	-	Artifacts
2005-10-31	ARDS_Rampe_1_01_.eit	Dur1.fpv	rampe1	-	Artifacts
2005-10-31	ARDS_Rampe_1b_01_.eit	Dur1b.fpv	rampe2	-	Artifacts
2005-10-31	ARDS_Rampe_2_01_.eit	Dur2.fpv	rampe3	-	Artifacts
2005-11-01	ARDS_Rampe_1_01_.eit	dur1.fpv	rampe1	-	Artifacts
2005-11-01	ARDS_Rampe_2_01_.eit	Dur2.fpv	rampe2	-	Artifacts
2005-11-01	ARDS_Rampe_2b_01_.eit	Dur2b.fpv	rampe3	-	Artifacts
2005-11-02	ARDS_Rampe_1_01_.eit	dur1.fpv	rampe1	-	OK [a]

[a] Downward PEEP titration has only 3 steps, therefore was not used.

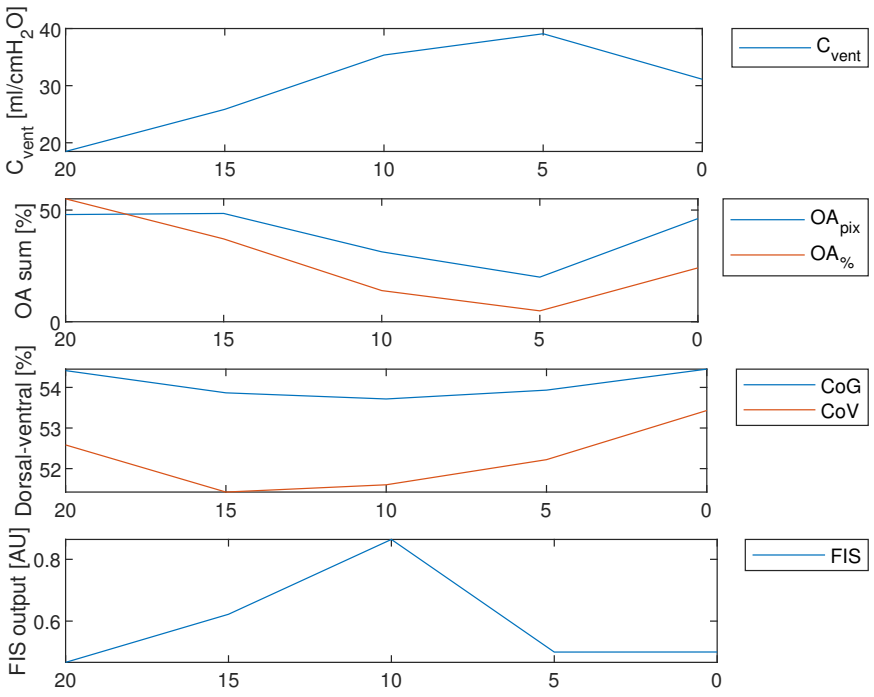

Figure A.1: Alignment of features and evaluation of FIS for subject A.

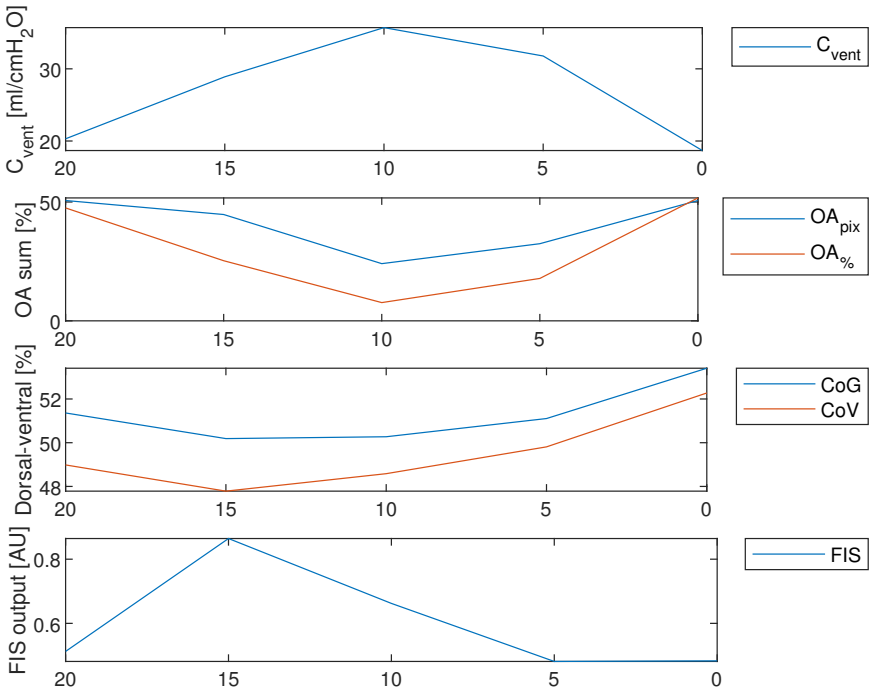

Figure A.2: Alignment of features and evaluation of FIS for subject B.

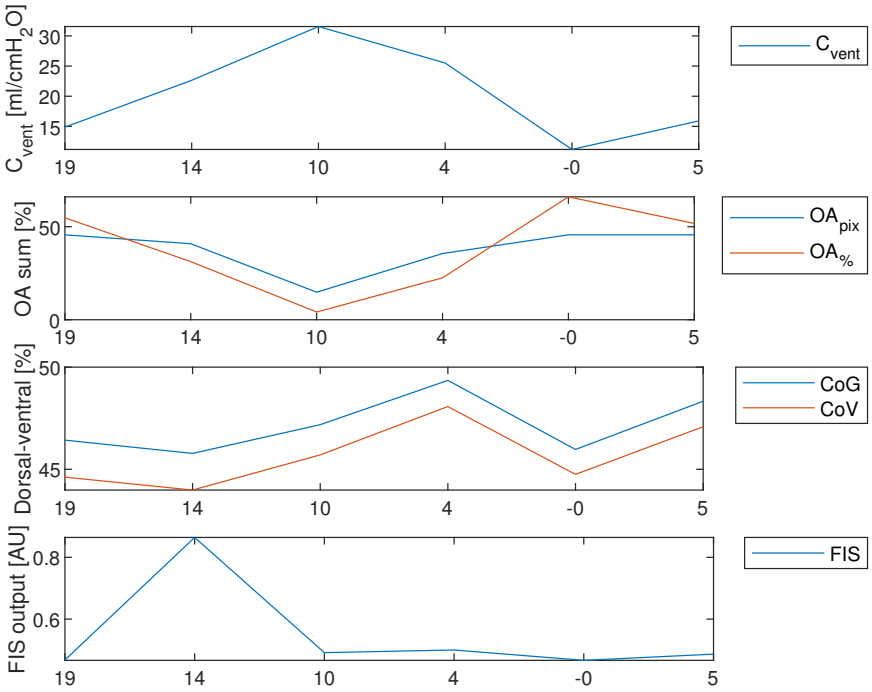

Figure A.3: Alignment of features and evaluation of FIS for subject C.

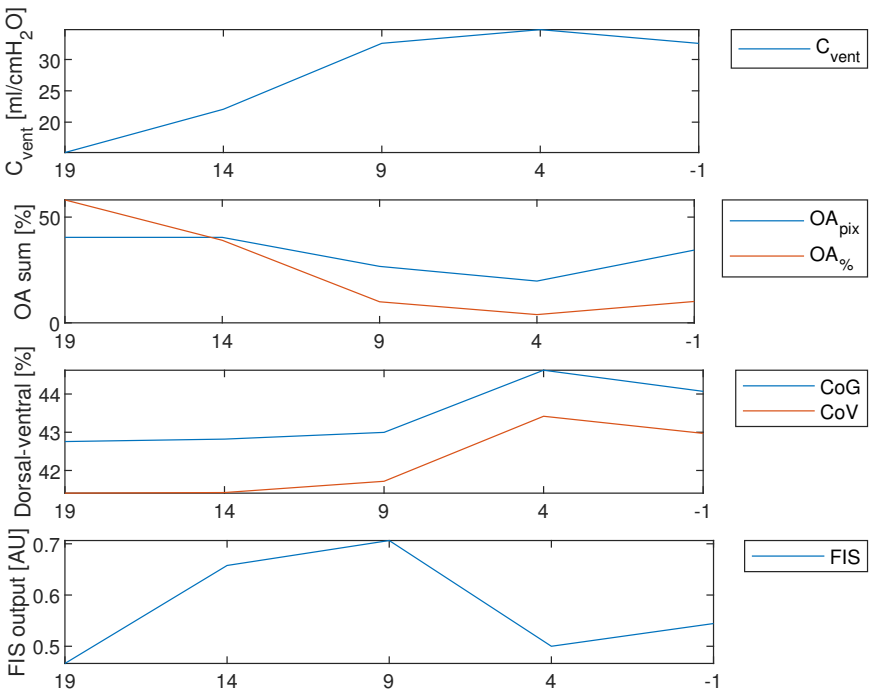

Figure A.4: Alignment of features and evaluation of FIS for subject D.

Bibliography

[1] H. J. H. Colebatch and C. K. Y. Ng. Estimating alveolar surface area during life. *Respiration Physiology*, 88(1):163–170, April 1992.

[2] Gary T. Ferguson. Why Does the Lung Hyperinflate? *Proceedings of the American Thoracic Society*, 3(2):176–179, April 2006. Publisher: American Thoracic Society - PATS.

[3] Jay P. Desai and Fady Moustarah. Pulmonary Compliance. In *StatPearls*. StatPearls Publishing, Treasure Island (FL), 2020.

[4] John E. Hall and Arthur C. Guyton. *Textbook of Medical Physiology*. Elsevier, Philadelphia, 14 edition, 2020.

[5] Pardis Ghafarian, Hamidreza Jamaati, and Seyed Mohammadreza Hashemian. A Review on Human Respiratory Modeling. *Tanaffos*, 15(2):61–69, 2016.

[6] J. Gordon Betts, Kelly A. Young, James A. Wise, et al. *Anatomy and Physiology*. OpenStax, Houston, Texas, April 2013.

[7] Esteban Ortiz-Prado, Jeff F. Dunn, Jorge Vasconez, et al. Partial pressure of oxygen in the human body: a general review. *American Journal of Blood Research*, 9(1):1, 2019. Publisher: e-Century Publishing Corporation.

[8] DavidG. Ashbaugh, D. Boyd Bigelow, ThomasL. Petty, et al. Acute Respiratory Distress in Adults. *The Lancet*, 290(7511):319–323, August 1967.

[9] G. R. Bernard, A. Artigas, K. L. Brigham, et al. Report of the American-European consensus conference on ARDS: Definitions, mechanisms, relevant outcomes and clinical trial coordination. *Intensive Care Medicine*, 20(3):225–232, March 1994.

[10] V. Marco Ranieri, Gordon D. Rubenfeld, B. Taylor Thompson, et al. Acute respiratory distress syndrome: the Berlin Definition. *JAMA*, 307(23):2526–2533, June 2012.

[11] Vito Fanelli, Aikaterini Vlachou, Shirin Ghannadian, et al. Acute respiratory distress syndrome: new definition, current and future therapeutic options. *Journal of Thoracic Disease*, 5(3):326–334, June 2013.

[12] Maurizio Zompatori, Federica Ciccarese, and Luca Fasano. Overview of current lung imaging in acute respiratory distress syndrome. *European Respiratory Review*, 23(134):519–530, December 2014. Publisher: European Respiratory Society Section: Series.

[13] Luciano Gattinoni and Antonio Pesenti. The concept of "baby lung". *Intensive Care Medicine*, 31(6):776–784, June 2005.

[14] Luciano Gattinoni, John J. Marini, Antonio Pesenti, et al. The "baby lung" became an adult. *Intensive Care Medicine*, 42(5):663–673, May 2016.

[15] Emanuele Rezoagli, Roberto Fumagalli, and Giacomo Bellani. Definition and epidemiology of acute respiratory distress syndrome. *Annals of Translational Medicine*, 5(14), July 2017.

[16] T. Pham, L. J. Brochard, and A. S. Slutsky. Mechanical Ventilation: State of the Art, September 2017. ISSN: 1942-5546 Issue: 9 Publisher: Mayo Clin Proc Volume: 92.

[17] W. Nikischin, T. Gerhardt, R. Everett, et al. A new method to analyze lung compliance when pressure-volume relationship is nonlinear, October 1998. ISSN: 1073-449X Issue: 4 Publisher: Am J Respir Crit Care Med Volume: 158.

[18] Steffen Leonhardt and Marian Walter, editors. *Medizintechnische Systeme: Physiologische Grundlagen, Gerätetechnik und automatisierte Therapieführung.* Springer Vieweg, 2016.

[19] H. Montgomery, L. Camporota, O. Orhan, et al. *The Intensive Care Foundation Handbook of Mechanical Ventilation: A User's Guide.* The Intensive Care Foundation, London, UK, 2015.

[20] Jason H. T. Bates and Bradford J. Smith. Ventilator-induced lung injury and lung mechanics. *Annals of Translational Medicine*, 6(19), October 2018. Publisher: AME Publications.

[21] D. Dreyfuss, P. Soler, G. Basset, et al. High inflation pressure pulmonary edema. Respective effects of high airway pressure, high tidal volume, and positive end-expiratory pressure. *The American Review of Respiratory Disease*, 137(5):1159–1164, May 1988.

[22] Jeremy R. Beitler, Atul Malhotra, and B. Taylor Thompson. Ventilator-Induced Lung Injury. *Clinics in chest medicine*, 37(4):633–646, December 2016.

[23] Anake Pomprapa, David Schwaiberger, Philipp Pickerodt, et al. Automatic protective ventilation using the ARDSNet protocol with the additional monitoring of electrical impedance tomography. *Critical Care*, 18(3):R128, 2014.

[24] H. Luepschen, T. Meier, M. Grossherr, et al. Protective ventilation using electrical impedance tomography. *Physiological Measurement*, 28(7):S247–S260, June 2007. Publisher: IOP Publishing.

[25] Alexandre Biasi Cavalcanti, Erica Aranha Suzumura, Ligia Nasi Laranjeira, et al. Effect of Lung Recruitment and Titrated Positive End-Expiratory Pressure (PEEP) vs Low PEEP on Mortality in Patients With Acute Respiratory Distress Syndrome: A Randomized Clinical Trial. *JAMA*, 318(14):1335, October 2017.

[26] Robert M. Kacmarek, Jesús Villar, Demet Sulemanji, et al. Open Lung Approach for the Acute Respiratory Distress Syndrome: A Pilot, Randomized Controlled Trial*. *Critical Care Medicine*, 44(1):32–42, January 2016.

[27] Joris Pensier, Audrey de Jong, Zied Hajjej, et al. Effect of lung recruitment maneuver on oxygenation, physiological parameters and mortality in acute respiratory distress syndrome patients: a systematic review and meta-analysis. *Intensive Care Medicine*, 45(12):1691–1702, December 2019.

[28] David Naranjo-Hernández, Javier Reina-Tosina, and Mart Min. Fundamentals, Recent Advances, and Future Challenges in Bioimpedance Devices for Healthcare Applications, July 2019. ISSN: 1687-725X Pages: e9210258 Publisher: Hindawi Volume: 2019.

[29] Andy Adler, Pascal Olivier Gaggero, and Yasheng Maimaitijiang. Adjacent stimulation and measurement patterns considered harmful. *Physiological Measurement*, 32(7):731–744, June 2011. Publisher: IOP Publishing.

[30] Eckhard Teschner, Michael Imhoff, and Steffen Leonhardt. *Electrical Impedance Tomography: The realisation of regional ventilation monitoring.* Drägerwerk AG & Co. KGaA, Lübeck, Germany, 2 edition, 2015.

[31] Xinying Zheng and Ge Kou. Research on EIT Image Reconstruction Based on Improved GREIT Algorithm. In *2019 IEEE International Conference on Signal, Information and Data Processing (ICSIDP)*, pages 1–4, December 2019.

[32] Andy Adler, John H. Arnold, Richard Bayford, et al. GREIT: a unified approach to 2D linear EIT reconstruction of lung images. *Physiological Measurement*, 30(6):S35–S55, June 2009. Publisher: IOP Publishing.

[33] L. A. Zadeh. Fuzzy sets. *Information and Control*, 8(3):338–353, June 1965.

[34] Elena Vlamou and Basil Papadopoulos. Fuzzy logic systems and medical applications. *AIMS Neuroscience*, 6(4):266–272, October 2019.

[35] Vladimir Sobota and Karel Roubik. Center of Ventilation—Methods of Calculation Using Electrical Impedance Tomography and the Influence of Image Segmentation. In *XIV Mediterranean Conference on Medical and Biological Engineering and Computing 2016*, pages 1258–1263. Springer, January 2016.

[36] Zhanqi Zhao, Li-Chung Lee, Mei-Yun Chang, et al. The incidence and interpretation of large differences in EIT-based measures for PEEP titration in ARDS patients. *Journal of Clinical Monitoring and Computing*, 34(5):1005–1013, October 2020.

[37] Eduardo L. V. Costa, João Batista Borges, Alexandre Melo, et al. Bedside estimation of recruitable alveolar collapse and hyperdistension by electrical impedance tomography. *Intensive Care Medicine*, 35(6):1132–1137, June 2009.

[38] Paul Blankman, Djo Hasan, Groot Jebbink Erik, et al. Detection of 'best' positive end-expiratory pressure derived from electrical impedance tomography parameters during a decremental positive end-expiratory pressure trial. *Critical Care*, 18(3):R95, May 2014.

[39] Zhanqi Zhao, Daniel Steinmann, Inéz Frerichs, et al. PEEP titration guided by ventilation homogeneity: a feasibility study using electrical impedance tomography. *Critical Care*, 14(1):R8, January 2010.